

# Hot gas in massive halos drives both mass quenching and environment quenching

J. M. Gabor,<sup>1</sup>\* R. Davé<sup>2,3,4</sup>

<sup>1</sup>CEA-Saclay, IRFU, SAp, F-91191 Gif-sur-Yvette, France

<sup>2</sup>University of the Western Cape, Bellville, Cape Town 7535, South Africa

<sup>3</sup>South African Astronomical Observatories, Observatory, Cape Town 7925, South Africa

<sup>4</sup>African Institute for Mathematical Sciences, Muizenberg, Cape Town 7945, South Africa

7 October 2018

## ABSTRACT

Observed galaxies with high stellar masses or in dense environments have low specific star formation rates, i.e. they are quenched. Based on cosmological hydrodynamic simulations that include a prescription where quenching occurs in regions dominated by hot ( $> 10^{5.4}$  K) gas, we argue that this hot gas quenching in halos  $> 10^{12} M_{\odot}$  drives both mass quenching (i.e. central quenching) and environment quenching (i.e. satellite quenching). These simulations reproduce a broad range of locally observed trends among quenching, halo mass, stellar mass, environment, and distance to halo center. Mass quenching is independent of environment because  $\sim 10^{12} - 10^{13} M_{\odot}$  “mass quenching halos” inhabit a large range of environments. On the other hand, environment quenching is independent of stellar mass because galaxies of all stellar masses may live in dense environments as satellites of groups and clusters. As in observations, the quenched fraction of satellites increases with halo mass and decreases with distance to the center of the group or cluster. We investigate pre-processing in group halos, ejected former satellites, and hot gas that extends beyond the virial radius. The agreement of our model with key observational trends suggests that hot gas in massive halos plays a leading role in quenching low-redshift galaxies.

**Key words:** galaxies:evolution – galaxies:formation

## 1 INTRODUCTION

It has long been recognized that the most massive galaxies as well as galaxies in dense regions have not formed substantial new stars for many Gyr. As a result they lie on a tight locus in color-magnitude space known as the red sequence. The mechanisms that halt star formation and cause the appearance of the red sequence of galaxies, often referred to as quenching, remain poorly understood. Observations imply that the red sequence noted at  $z = 0$  (e.g. Strateva et al. 2001) is already well-established by  $z = 1$  (e.g. Bell et al. 2004; Arnouts et al. 2007; Faber et al. 2007) and even earlier at  $z \sim 2$  (Williams et al. 2009; Brammer et al. 2009, 2011; Whitaker et al. 2013) to  $z \sim 4$  (Ilbert et al. 2013; Muzzin et al. 2013; Straatman et al. 2013). Deep surveys enable careful accounting of the growth of the red sequence over cosmic time. Combined with the present-day age of the stellar population in red sequence galaxies, this suggests that they must have built up mass through star-formation at an early epoch, and then some process(es) quenched their star formation.

A common theoretical explanation for quenching is that massive halos above  $\sim 10^{12} M_{\odot}$  form hot gas coronae via the virial

shock (Birnboim & Dekel 2003; Kereš et al. 2005), and this hot gas fails to cool, thus starving galaxies of fuel for star-formation (Dekel & Birnboim 2006; Cattaneo et al. 2006; Birnboim et al. 2007). The virial shock heats any gas inflows from the inter-galactic medium (IGM), preventing that inflowing gas from directly feeding the galaxies. In many circumstances the hot gas is expected to eventually cool in a so-called cooling flow (e.g. Fabian et al. 1984), so an additional heating source is required to prevent such cooling and resulting star-formation (Croton et al. 2006; Bower et al. 2006; Somerville et al. 2008, e.g.). This general class of quenching model is sometimes called halo quenching, owing to the dependence on halos above  $10^{12} M_{\odot}$ ; or radio mode AGN feedback (Croton et al. 2006), owing to the invocation of radio AGN as the heating source; or maintenance mode feedback, because an AGN only needs to maintain the high temperature of the halo gas rather than heat it from cold to hot. We prefer “hot halo” quenching because we will argue that the hot gaseous halo is the key ingredient.

Depending on their density structure, some hot halos may naturally have cooling times longer than the Hubble time, so no feedback effects are needed to quench star-formation (Kereš et al. 2009a). Furthermore, unresolved gravitational heating may provide sufficient thermal energy to maintain hot halos without the need for black hole feedback (Dekel & Birnboim 2008; Johansson et al.

\* Email:jared.gabor@cea.fr

2009; Birnboim & Dekel 2011; Feldmann et al. 2011). The details of heating and cooling of hot gas in massive halos are not fully understood (De Lucia et al. 2010), but models where hot gaseous halos are assumed to stay hot can successfully produce a realistic red sequence (Gabor et al. 2011).

Observed correlations between quenched galaxies and stellar mass, morphology, and environment offer clues to their formation mechanisms (e.g. Blanton & Moustakas 2009 for a review for local galaxies; Elbaz et al. 2007, Cooper et al. 2007, and Quadri et al. 2012 for environmental effects at  $z \approx 1 - 2$ ). Recent work has revealed trends suggesting two distinct quenching modes – “mass quenching” and “environment quenching” (Peng et al. 2010). These appear distinct because galaxies are increasingly likely to be quenched at high stellar masses, independent of environment (mass quenching), and galaxies are increasingly likely to be quenched in dense environments, independent of stellar mass (environment quenching). Peng et al. (2012) argue that environment quenching applies mainly to satellite galaxies, and appears independent of halo mass. Based on these local trends, they suggest that a quenching model based on halo mass is problematic. Knobel et al. (2013) suggest that these trends persist out to  $z \sim 1$ . Woo et al. (2013) reframed satellite quenching by considering distance to the halo center, and argue that halo quenching models could explain the results.

In this work we use cosmological hydrodynamic simulations to show how quenching associated with hot halo gas drives the observed trends. Specifically, both mass quenching and environment quenching emerge from the same simple quenching model, where galaxies in hot halos are quenched. Because the presence of hot gas is closely tied to halo masses  $> 10^{12} M_{\odot}$  (e.g. Birnboim & Dekel 2003; Kereš et al. 2005; Gabor et al. 2010), this implies that “halo quenching” models remain viable.

We describe our simulations in §2, including details of our quenching model in §2.1. Our simulation methodology is based on that in Gabor & Davé (2012), but we use a larger simulation volume. With this larger simulation we extend our previous analysis of the growth of the red sequence to explore the relationships between hot gas and environment. Inspired by observations, we illustrate various trends among quenching, halo mass, stellar mass, and environment, in §3. These trends include the red fraction as a function of environment and stellar mass, the stellar mass – halo mass relation for centrals and satellites, and the invariance of star-forming galaxy stellar mass functions with halo mass. In §4 we lay out a quenching narrative for galaxies in different halos, and we conclude with §5.

## 2 SIMULATIONS

The basic methodology of the simulations used here is identical to that in Gabor & Davé (2012), albeit with larger volumes. We summarise the simulations here.

We use a modified version of the publicly-available Smoothed Particle Hydrodynamics code GADGET-2 (Springel 2005) to solve N-body gravitational dynamics and the equations of hydrodynamics starting from cosmological initial conditions. We include a model for gas cooling and photoionization from a meta-galactic UV background Sutherland & Dopita (1993); Haardt & Madau (2001). We track chemical evolution of gas and stars through four metal species and our cooling function incorporates metal-line cooling appropriate for each gas particle’s metallicity (Oppenheimer & Davé 2008).

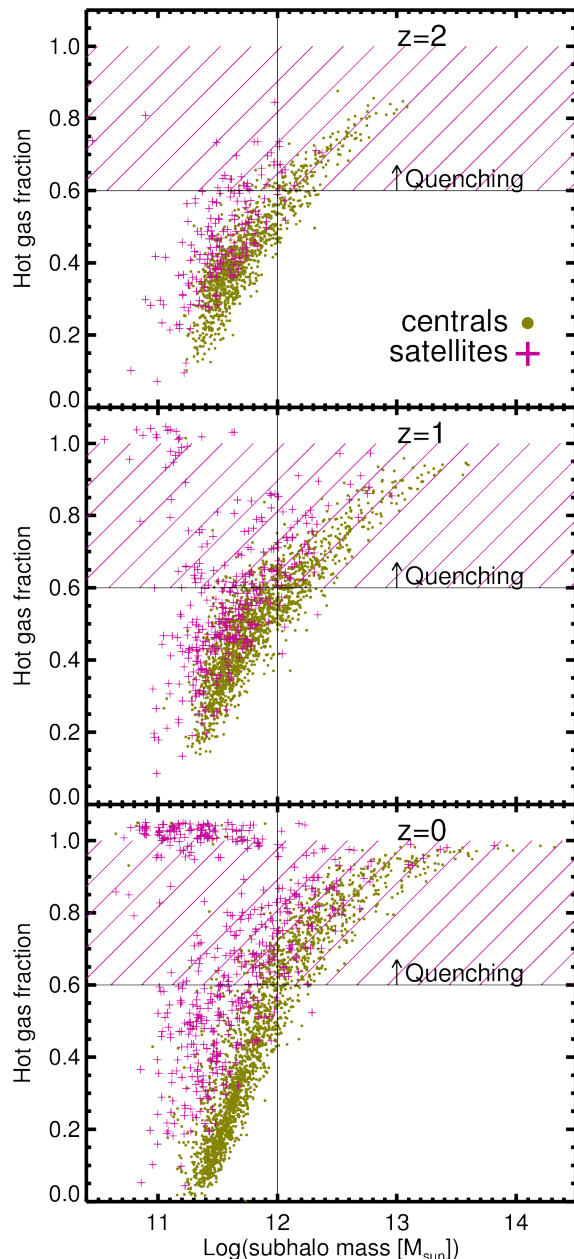


**Figure 1.** Hot gas fraction  $f_{\text{hot}}$  vs. subhalo mass at  $z = 2, 1,$  and  $0$  (top to bottom). Thin black lines mark  $M_{\text{halo}} = 10^{12} M_{\odot}$  and  $f_{\text{hot}}$  for visual reference. For centrals (green circles), hot gas fraction correlates well with halo mass, and halos above  $\sim 10^{12} M_{\odot}$  are dominated by hot gas. Many satellite galaxies (purple crosses) are dominated by hot gas despite low subhalo masses – these generally have massive parent halos that contain hot gas (we add a small amount of scatter to satellites with  $f_{\text{hot}} = 1$  for clarity). The trends show little variation with redshift. In our quenching model, we prevent gas accretion onto galaxies with  $f_{\text{hot}} > 60\%$ , as indicated by diagonal hatching.

Gas that collapses into structures denser than a threshold of  $0.13 \text{ cm}^{-3}$  is governed by the 2-phase star-formation model of (Springel & Hernquist 2003), based on (McKee & Ostriker 1977). This single-parameter model is tuned to match the Kennicutt star-formation relation (Kennicutt 1998). Star-forming gas particles self-enrich with metals from supernovae, and stochastically spawn

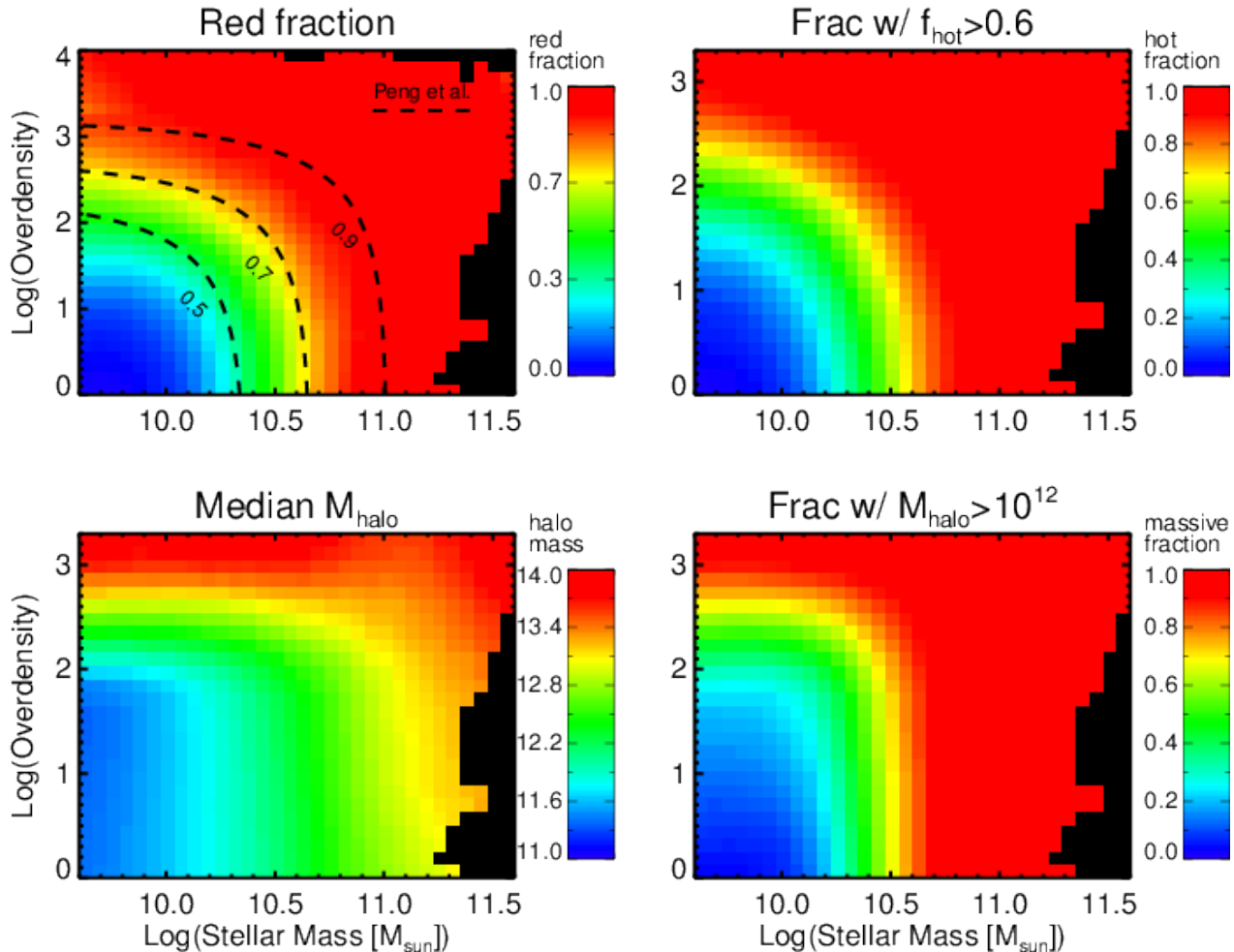


**Figure 2.** The appearance of mass quenching and satellite quenching in our simulations: as a function of 5th-nearest neighbor overdensity (see §2.3) and stellar mass, we plot (in color) the fraction of galaxies that are quenched (**top left**), the fraction of galaxies whose *subhalo* is dominated by hot gas (**top right**), the median parent halo mass (**bottom left**), and the the fraction of galaxies with a parent halo mass above  $10^{12} M_{\odot}$  (**bottom right**). The boxy shape of the contours in observations of the red fraction (cf. dashed lines in top left panel) led Peng et al. (2010) to conclude that mass quenching and environment quenching are distinct processes. This figure shows that, in our hot gas quenching model, the boxy pattern appears with parent halo mass as well. Mass quenching and environment quenching are two manifestations of quenching in hot, massive halos.

collisionless star particles as well as ejecting galactic winds. During each time step, each star-forming gas particle spawns a new star particle with a probability consistent with its star-formation rate. The typical mass of the star particles thus spawned is roughly half the gas particle mass, so that gas particles generally may spawn two star particles.

After formation, star particles lose mass and metals due to AGB feedback and Type Ia supernovae. We calculate evolved stellar mass loss using stellar population models (Bruzual & Charlot 2003), and spread the lost mass to nearby gas particles. Type Ia SN rates are taken from (Scannapieco & Bildsten 2005), and these inject both mass and energy into the surrounding gas.

Star-forming gas particles may also be launched in a galactic wind. We assume the wind mass outflow rate,  $\dot{M}_{\text{wind}}$ , is proportional to the star-formation rate divided by the galaxy circular velocity. In order to calculate circular velocities, we use an on-the-fly friends-of-friends (FoF) galaxy-finder to estimate galaxy masses. During each time step, each star-forming gas particle has a probability of being launched in a wind that is consistent with

$\dot{M}_{\text{wind}}$ . New wind particles are given a kick velocity  $v_{\text{wind}}$  proportional to the galaxy circular velocity, and they are decoupled from the normal hydrodynamics until the local density has dropped to one-tenth the star-formation threshold density, for up a time up to  $20 \text{ kpc}/v_{\text{wind}}$ . The scalings of  $\dot{M}_{\text{wind}}$  and  $v_{\text{wind}}$  with the SFR and circular velocity are motivated by the theory of momentum-conserving winds (Murray et al. 2005, 2011), which in turn is motivated by local observations of starburst galaxies (Rupke et al. 2005; Martin 2005). These wind scalings lead to star-forming galaxies and inter-galactic medium properties that match a wide variety of observational constraints (Oppenheimer & Davé 2006; Finlator et al. 2006; Davé et al. 2007; Finlator et al. 2007; Finlator & Davé 2008; Davé et al. 2008; Oppenheimer & Davé 2008, 2009; Oppenheimer et al. 2009; Davé et al. 2011b,a; Oppenheimer et al. 2012).

Simulations using our favoured wind model reproduce the observed number densities of low-mass star-forming galaxies, but they generally over-produce massive galaxies. In part to remedy this problem, we developed a quenching model for our simulations, as discussed next.

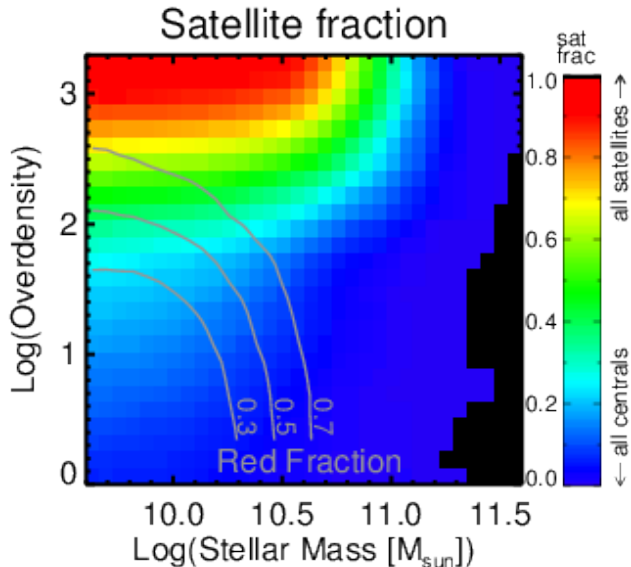


**Figure 3.** Satellite fraction (colors) as a function of environment and stellar mass. Satellite fraction is calculated in each pixel  $i$  (i.e. each 2-dimensional bin of overdensity and stellar mass) as  $f_{\text{sat},i} = N_{\text{sat},i}/N_{\text{tot},i}$ , where  $N_{\text{sat},i}$  is the number of satellite galaxies falling in pixel  $i$  and  $N_{\text{tot},i}$  is the total number of galaxies (centrals plus satellites) falling in pixel  $i$ . Gray lines show contours of red (i.e. quenched) fraction from Figure 2. This shows that environment quenching is mainly associated with satellite galaxies, while mass quenching is associated with centrals.

## 2.1 Quenching in hot halos

We quench star-formation by adding thermal energy to hot halos in our simulations. Hydrodynamic calculations robustly predict the formation of a stable “virial shock” in dark matter halos (only) above a mass  $\sim 10^{12} M_{\odot}$  (e.g. Birnboim & Dekel 2003; Kereš et al. 2005; Gabor et al. 2010). This virial shock heats the gas in the halo from typical IGM temperatures of  $10^4$  K to  $> 10^5$  K. While the hot gas overall has long cooling times, in the central regions it typically cools and fuels star formation in simulations. In Figure 1 we show the hot gas fraction as a function of subhalo mass in one of our simulations *without* quenching. The hot gas fraction for central galaxies rapidly increases around halo masses of  $10^{12} M_{\odot}$ . The relationship is fairly tight, but at a fixed hot fraction there is scatter of at least a tenth of a decade in subhalo mass. Satellite galaxies often live in the hot gas environment of their more massive host halos, so that their local hot gas fraction is decoupled from their subhalo mass.

Additional heating sources such as radio AGN (Croton et al. 2006; Somerville et al. 2008), cosmic rays (Mathews 2009), or unresolved gravitational heating (Dekel & Birnboim 2008; Johansson et al. 2009; Birnboim & Dekel 2011) may act to heat the gas and prevent it from cooling, thus starving galaxies in the centers of hot halos of fuel for star-formation. Other processes such as ram pressure stripping (Gunn & Gott 1972) may help quench satellite galaxies. Our quenching model is designed to emulate this heating in hot halos, while remaining agnostic regarding its physical origin. Our basic approach is to identify galaxies living in hot halos, then continuously heat the nearby circum-galactic medium around those galaxies to prevent it from cooling and forming stars.

We identify hot halos on-the-fly by exploiting the FoF galaxy finder. The FoF galaxies generally include the stars and star-

forming gas as well as a small fraction of the immediate circum-galactic (non-star-forming) gas. For each identified FoF galaxy, we estimate the dark matter subhalo mass and virial radius by scaling the mass from the FoF algorithm. We count up all gas particles within that virial radius, and calculate the fraction that is hotter than  $10^{5.4}$  K. We take this value from Kereš et al. (cf. 2005), who found that the gas flowing into simulated galaxies has a temperature distribution with a local minimum at this critical temperature, corresponding to a local minimum in the cooling curve that separates free-free emission from helium cooling. If the hot gas fraction is above 0.6, we consider the galaxy to be embedded in a hot halo. We initially chose the critical hot fraction of 0.6 to match the hot fraction in the average  $10^{12} M_{\odot}$  halo, as in Figure 1, and we have not tuned it to match any observables. Experiments with higher critical hot fractions (e.g. 0.7) show that these allow the formation of more massive galaxies, but too few low and moderate-mass galaxies are quenched. In galaxies embedded in a hot halo, we heat the circum-galactic gas to the virial temperature. We do not add heat to the star-forming gas, and we do not add heat throughout the halo – we only heat gas identified by the FoF galaxy finder. We heat these gas particles at every time step, using arbitrary amounts of thermal energy to keep them at the virial temperature.

Recent cosmological simulations using the moving mesh code AREPO (cf. Springel 2010) suggest that the nature of galaxy fueling depends on hydrodynamic method. At late times, moving-mesh simulations tend to show more cooling in massive halos than do SPH simulations (Kereš et al. 2012; Vogelsberger et al. 2012), probably owing to inaccuracies in standard SPH formulations (Hayward et al. 2014). Contrary to previous results, the majority of the gas fueling galaxies in AREPO simulations passes through a hot phase (Nelson et al. 2013). The full implications of this difference have only begun to be explored (Vogelsberger et al. 2013; Torrey et al. 2014), but the appearance of stable hot halos seems to be mostly unchanged in these simulations. In Nelson et al. (2013), hot halos develop at halo masses  $< 10^{12} M_{\odot}$  in both moving mesh and GADGET simulations, but this is lower than in our simulations partly because they do not include the effects of metal line cooling (and hence are more in line with Kereš et al. 2005). We therefore suspect that uncertainties related to the hydrodynamic method will have only a minor impact on our simple quenching model. Although the different methods lead to different temperature and density distributions of gas within halos (Kereš et al. 2012), they apparently do not drastically change *which* halos are hot. Our quenching model triggers based on the latter. Ongoing tests with revised formulations of SPH which improve its accuracy (Saitoh & Makino 2013; Hopkins 2013) should address this uncertainty more directly.

By heating the circumgalactic gas around galaxies living in hot halos, our quenching model effectively starves or strangles galaxies by cutting off the fuel for star-formation. In our model the mechanism works similarly for central and satellite galaxies. Once galaxies are embedded in a hot halo, they may continue to form stars until they exhaust their existing reservoir of gas. This allows some satellite galaxies to survive as star-forming even as they fall through a hot halo and merge with the central galaxy. In some cases, as discussed later, this leads to “rejuvenation,” where a satellite galaxy delivers a new supply of star-forming gas to its central galaxy, turning a quenched central into a star-forming one (for a brief time). Rejuvenated galaxies generally grow very little in mass through the added star-formation, but they can temporarily become green valley galaxies.

This simple hot gas quenching model produces a realistic  $z = 0$  red sequence, with galaxy number densities matching local obser-

vations (Gabor et al. 2011). Central galaxies with stellar masses  $\gtrsim 10^{10.5} M_{\odot}$  are the first to be quenched at  $z > 2$  because their halos are dominated by hot gas at high redshift. After joining the red sequence they continue to accrete satellites and may grow in mass by factors of 2 or more by  $z = 0$ . Satellites continually join these massive halos and are also quenched, filling in lower masses on the red sequence, especially at  $z < 1$ . Concurrently, new massive star-forming galaxies are quenched as their halos grow to  $> 10^{12} M_{\odot}$  down to  $z = 0$  (Gabor & Davé 2012).

We note that in our simulations, mergers generally do not cause quenching. Our hot gas quenching model is not explicitly linked to galaxy mergers, and in our simulations without hot gas quenching, mergers produce very few red galaxies. This result contrasts with some popular quenching models (e.g. Hopkins et al. 2006, 2008). In Gabor et al. (2011) we showed that a separate quenching model based on major mergers does not produce enough quenched galaxies, primarily because merger remnants continue to accrete new fuel for star-formation even if they eject all their pre-merger gas.

In Gabor et al. (2011) and Gabor & Davé (2012) we identified some weaknesses of this quenching model. Starvation due to the presence of hot gas alone has difficulty creating sufficient numbers of massive quenched galaxies at  $z \gtrsim 2$ . This is partly because the timescale for gas starvation is a significant fraction of the age of the universe at very high  $z$ . Thus a faster-acting quenching (such as galaxy mergers or violent disk instabilities) may be required in combination with starvation in the early universe. Another problem is that our model with hot gas quenching produces too few massive star-forming galaxies, suggesting that this quenching is too efficient – that is, hot gas quenching shuts down SF in *all* massive galaxies, whereas a better model would shut down SF in *most*, but not quite all such galaxies. In simulations without quenching (but with stellar-driven winds), the high- $z$  stellar mass function for all galaxies is in good agreement with observations. The addition of a quenching model can only lower galaxy masses. Thus, in order for a model with quenching to get enough high-mass, high- $z$  galaxies, the stellar feedback efficiency probably should be lowered so that massive galaxies can acquire more mass before they are quenched. Despite these difficulties, hot gas quenching appears to be a good model for the low- $z$  red sequence. The problems noted above primarily apply to high- $z$  galaxies, while most of the red sequence is built up at  $z < 1$  (e.g. Faber et al. 2007).

In summary, our quenching model prevents gas accretion onto galaxies that live in regions dominated by hot gas, which typically arise in halos with masses above  $10^{12} M_{\odot}$ . Such galaxies are effectively starved of new fuel for star-formation, and they fade to red as they exhaust their remaining cold gas reservoir.

## 2.2 Simulation runs

For the remainder of the paper, we focus on simulations using our quenching model (along with all the other physical processes above). Our main simulation was run in a periodic cubic box with a side length of  $96h^{-1}$  Mpc, with  $512^3$  dark matter particles and  $512^3$  initial gas particles. This simulation allows us to model massive structures such as several galaxy clusters with total  $z = 0$  masses a few  $\times 10^{14} M_{\odot}$ . For convenience of analysis or clarity of presentation, we also sometimes use smaller simulations with the same resolution: we use both a  $48h^{-1}$  Mpc box with  $2 \times 256^3$  particles, and a  $24h^{-1}$  Mpc box with  $2 \times 128^3$  particles, as noted in the text. We also make use of simulations with different sub-grid physics: we have already mentioned a simulation without quenching in §2.1

(which was run in a  $48h^{-1}$  Mpc box), and we also use a simulation that includes neither quenching nor stellar-driven winds (also  $48h^{-1}$  Mpc).

The effective spatial resolution, set by the softening length, is  $3.75h^{-1}$  kpc, and the mass of a gas particle is  $1.2 \times 10^8 M_{\odot}$ . We consider galaxies resolved if they contain at least 64 star particles, or a stellar mass  $\gtrsim 10^{9.5} M_{\odot}$ . Finlator et al. (2006) showed that this particle number criterion leads to converged star-formation histories, at least for star-forming galaxies in similar simulations. Our own convergence tests with  $\sim 3$  times better resolution than our main run (but which are run with smaller volumes and which do not proceed all the way to  $z = 0$ ) show that our results are not sensitive to resolution. The hot halos that drive our quenching model are sufficiently massive that they are always well-resolved.

All simulations use a WMAP5 cosmology with  $H_0 = 70 \text{ km s}^{-1} \text{ Mpc}^{-1}$ ,  $\Omega_{\text{matter}} = 0.28$ ,  $\Omega_{\text{baryon}} = 0.046$ ,  $\Omega_{\Lambda} = 0.7$  (Komatsu et al. 2009). We output  $\approx 100$  simulation snapshots between  $z = 10$  and  $z = 0$ , with a time between consecutive snapshots of  $\sim 100 - 300$  Myr. For most of this work, we focus on trends in the local universe, so we use a snapshot at  $z = 0.025$  which is comparable to local observational samples from e.g. SDSS (Blanton et al. 2005). We will typically refer to this as  $z = 0$ .

## 2.3 Analysis methods

Once a simulation has run, we use a suite of tools to extract and analyze galaxy properties. We first identify galaxies and determine basic properties (e.g. stellar mass) and derived properties (e.g. absolute magnitudes). Then we identify dark matter halos in which the galaxies live, along with gas properties inside those halos. Finally, we quantify the large-scale environment around each galaxy.

We identify galaxies using SKID, which relies on the DENMAX algorithm to associate bound gas and star particles as galaxies. The galaxy stellar mass is the sum of the masses of the constituent star particles, the star-formation rate is the sum of the instantaneous SFRs of each gas particle, etc. We determine galaxy absolute magnitudes by considering each star particle as a single stellar population with a given age and metallicity, assigning each particle a spectrum based on a stellar population model (Bruzual & Charlot 2003), adding the spectra of all the star particles in the galaxy, and convolving that spectrum with various filters (e.g. the SDSS ugri filters).

We use “red” and “quenched” interchangeably to refer to galaxies with low specific star formation rates in our simulations. Simulated galaxies are classified as either red or blue based on their locations in an intrinsic absolute  $g - r$  color-vs-stellar mass diagram – we use a mass-dependent color cut that varies with redshift (see Gabor et al. 2011; Gabor & Davé 2012). We do not model the reddening due to dust, so galaxies on our red sequence are intrinsically red and thus have little star-formation. In fact, owing to our quenching model, most of the red galaxies in our simulations have zero instantaneous star formation rates.

We identify subhalos around each SKID galaxy, along with parent or host halos, using a spherical overdensity algorithm. We use “subhalo” to refer to matter that is within the virial radius of each galaxy. We use “parent halo” or “host halo” or just “halo” to refer to the largest halo in which a galaxy resides. Every galaxy has both a subhalo and a host halo – for central galaxies, the two are essentially the same. We first associate every particle in a simulation to the SKID galaxy to which it is most bound. Then, starting from each galaxy position, we iteratively step out in radius and count up the mass of associated particles within the sphere defined by that

radius until the average density within that subhalo falls below a redshift-dependent virial density appropriate for our assumed cosmology as given in Davé et al. (2010,  $\approx 100\times$  the critical density). This defines the virial radius, and mass, of the subhalo. We then “merge” subhalos. Subhalos that lie within the virial radius of a larger subhalo are subsumed into the larger halo – the smaller subhalo is now considered a satellite of the larger. From the association of subhalos to larger halos, we can identify groups and clusters of galaxies.

We measure the gas properties within each subhalo. For the hot gas fraction we simply add up the mass of hot gas within the subhalo virial radius and divide by the total gas mass:  $f_{\text{hot}} = M_{\text{gas}, > 10^{5.4} K} / M_{\text{gas}}$ . This gives a measure of hot gas fraction that is *local* to each galaxy, and enables a distinction between the local hot gas fraction around a satellite galaxy and the hot gas fraction of the parent galaxy cluster in which it lives. We also measure radial profiles of hot gas fraction and gas temperature for each subhalo.

We quantify galaxy environment using a 5th-nearest neighbor approach akin to that used by observers (Dressler 1980; Cooper et al. 2005, 2006; Kovač et al. 2010; Peng et al. 2010). We use all resolved galaxies ( $M_{\text{stellar}} > 10^{9.5} M_{\odot}$ ) to sample the density field. The overdensity at any point in the simulation box is  $\delta = (\rho_5 - \hat{\rho}) / \hat{\rho}$ , where  $\rho_5 = 5 / ((4/3)\pi R_5^3)$ ,  $R_5$  is the distance from the point to the 5th-nearest (resolved) neighbor galaxy, and  $\hat{\rho}$  is the average density of resolved galaxies in the entire simulation box,  $N_{\text{galaxies}} / (\text{simulation volume})$ . In figures we generally plot  $\log(1 + \delta)$  and denote this quantity as  $\log(\text{overdensity})$ . Note that we use a 3-dimensional 5th-nearest neighbor, whereas observers are generally restricted to projected measures. Our tests show that trends remain unchanged by this choice, but that a 3D measure better separates galaxies in the densest environments (see also Cooper et al. 2005).

We trace the histories of halos and galaxies using a progenitor-finding algorithm. Consider two output snapshots, 1 and 2, at redshifts  $z_1$  and  $z_2$  such that  $z_1 < z_2$ . We seek the most massive progenitor to halo  $H_1$  at  $z_2$ . For each dark matter particle in halo  $H_1$ , we find the halo in which it lived at  $z_2$  (if any). Among these halos at  $z_2$ , the most massive one is considered the main progenitor,  $H_2$ . We follow a similar procedure for star particles to identify the most massive progenitor of each galaxy. By comparing the  $z = 0$  snapshot to each previous snapshot, we construct the history of each galaxy and halo from  $z = 0$  to  $z \approx 6$ .

### 3 HOT GAS QUENCHING TRENDS

In this section we illustrate the crucial trends among stellar mass, halo mass, environment, hot gas, and quenching that emerge from our quenching model. Many of these match the observed trends. We emphasize that both mass quenching and environment quenching emerge naturally from our hot gas quenching model (Gabor & Davé 2012).

#### 3.1 The appearance of mass quenching and environment quenching

Figure 2 illustrates relationships among galaxy stellar mass, environment, halo mass, hot gas fraction, and red fraction in our model. In the top left panel we show the fraction of galaxies that are red (that is, quenched) as a function of environment and stellar mass (cf. Figure 7 of Gabor & Davé 2012). We compare with observational results by overplotting contours from an adjusted version of

the fitting function from equation 7 of Peng et al. (2010). Here overdensity is a 3-dimensional 5th-nearest-neighbor measure, whereas observations are restricted to projected measures. We adjust the best-fitting critical overdensity that appears in the Peng et al. (2010) fitting function as follows. First, we measure projected overdensities in our simulation (as in Gabor & Davé 2012), then fit a line to the relationship between our projected and 3D measures. Based on this best-fit line, the critical (logarithm of) overdensity of 1.84 becomes 2.57 when using a 3D density measure. The resulting contours are shown in Figure 2.

A characteristic boxy pattern emerges in the contours of red fraction, identical to that arising in observations (Peng et al. 2010). Galaxies with high stellar masses are more likely to be quenched, independent of environment, and galaxies in denser environments are more likely to be quenched, independent of stellar mass. Based largely on this boxy pattern, Peng et al. (2010) argue that mass quenching and environment quenching are separable, and therefore physically distinct processes. Furthermore, some authors suggest that environment quenching is decoupled from halo mass, since it appears to be independent of stellar mass in this figure.

The top right panel of Figure 2 shows the fraction of galaxies whose subhalo is dominated by hot gas (with  $f_{\text{hot}} > 0.6$ ). This panel shows the same boxy contours as that for red fraction, exactly as expected since our quenching model is directly tied to hot gas.

The bottom left panel of Figure 2 shows the median parent halo mass of galaxies in each bin of stellar mass and environment.  $M_{\text{halo}}$  generally increases with increasing overdensity, but only at overdensities above  $\sim 2$ . Below that overdensity,  $M_{\text{halo}}$  generally increases with stellar mass. Galaxies in massive groups and clusters with  $M_{\text{halo}} > 10^{13} M_{\odot}$  typically live in the highest-density regions, but some massive galaxies live in  $\sim 10^{13} M_{\odot}$  groups at low overdensities. That is, galaxies in halos with  $M_{\text{halo}} \approx 10^{13} M_{\odot}$  live in the full range of environments. We return to this point in §3.4.

The bottom right panel of Figure 2 shows the parent halo mass in a different way – it shows the fraction of galaxies whose parent halo is above  $10^{12} M_{\odot}$ . Here, a similar boxy pattern emerges as in the top two panels. Thus, the appearance of separable mass quenching and satellite quenching can emerge as a direct consequence of a critical halo mass (here  $\sim 10^{12} M_{\odot}$ ) where galaxies become quenched.

In summary, quenching in hot, massive halos naturally leads to the appearance of both mass quenching and environment quenching. The two quenching modes are in fact manifestations of the same process in our model. Despite our unified quenching mechanism, these appear to be mathematically separable as defined by Peng et al. (2010). The separability arises because massive halos which host massive central galaxies (e.g.  $M_{\text{halo}} > 10^{12}$  for  $M_{\text{stellar}} > 10^{10.5} M_{\odot}$ ) inhabit nearly the full range of environments, and galaxies in the densest environments may have a wide range of stellar masses.

#### 3.2 Mass quenching is central quenching; Environment quenching is satellite quenching

The observed mass quenching is mainly thought to be a result of quenched central galaxies, whereas environment quenching is the result of quenched satellites (e.g. Peng et al. 2012; Woo et al. 2013; see also e.g. De Lucia et al. 2012). Figure 3 shows that this is the case for our model. The galaxies with high red fraction at low  $M_{\text{stellar}}$  and high overdensity (i.e. towards the upper left of the figure) are satellite galaxies. Red galaxies with high  $M_{\text{stellar}}$  but low overdensities (towards the lower right) are centrals. Massive galax-

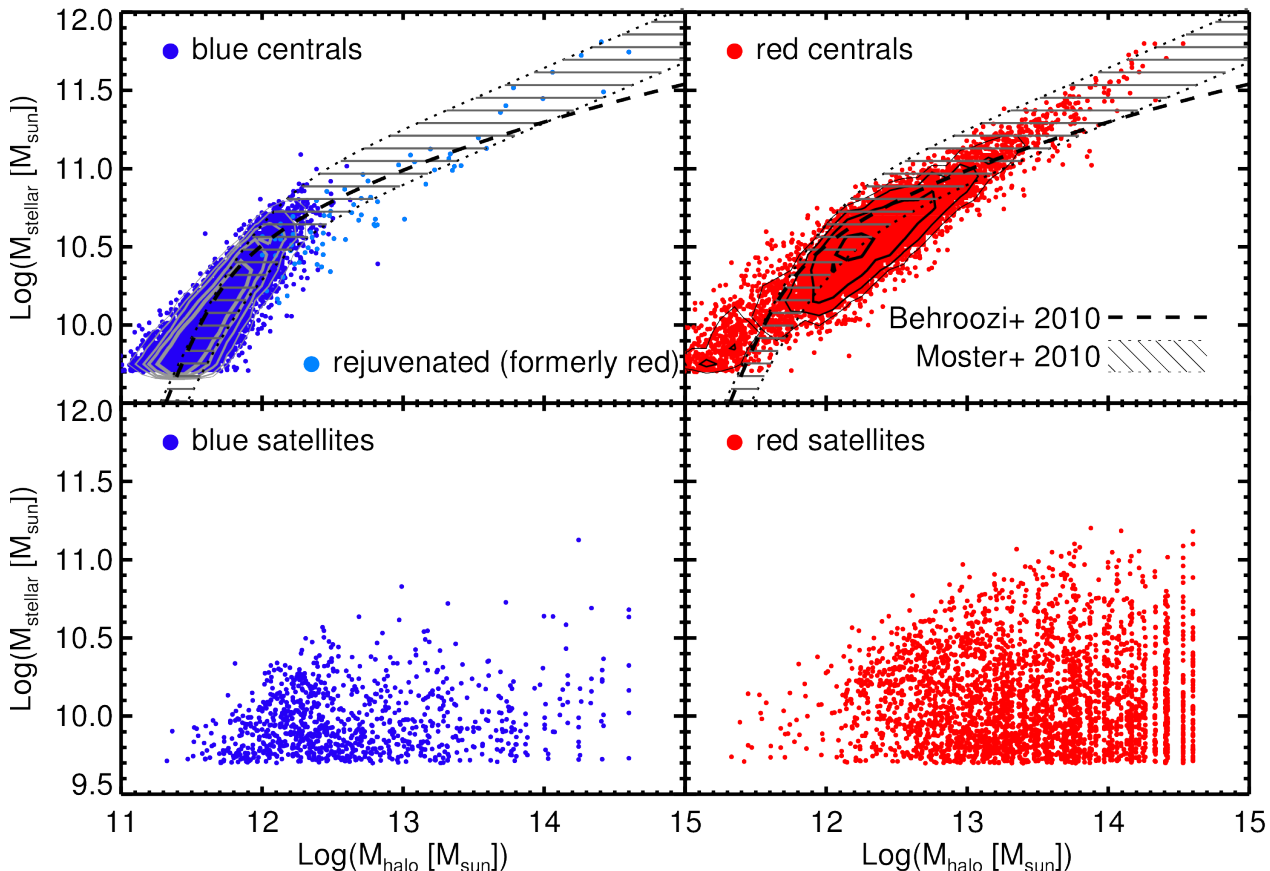


**Figure 4.** Stellar mass as a function of host halo mass, separated into red/blue and centrals/satellites, as labelled in each panel. For both blue centrals and red centrals (top row), stellar mass correlates strongly with halo mass, though the slope of the correlation for blue galaxies differs from that for red galaxies. The hatched region (Moster et al. 2010) and dashed line (Behroozi et al. 2010) show abundance matching constraints. For satellite galaxies (bottom row), stellar mass does not correlate with halo mass.

ies in dense environments (upper right) can be either centrals or satellites.

### 3.3 $M_{\text{stellar}} - M_{\text{halo}}$ relations

The stellar mass-halo mass relation is widely used to quantify the efficiency with which halos of different masses convert their baryons into stars (e.g. Mandelbaum et al. 2006; Conroy et al. 2007). It is closely linked to stellar mass function measurements through abundance-matching techniques (e.g. Moster et al. 2010; Behroozi et al. 2010), and has been well-studied especially in the  $z < 1$  universe with additional constraints from galaxy lensing and clustering (e.g. Leauthaud et al. 2012a,b; Tinker et al. 2013). Under the assumption that our understanding of dark matter structure formation is good, the stellar mass-halo mass relation serves as an important constraint on baryonic physics.

In our hot gas quenching model, star-forming central galaxies build up both halo mass and stellar mass over time as they accrete dark matter and gas. During this phase, galaxies accrete intergalactic gas without the hindrance of a hot halo, although their efficiency of converting baryons into stars is suppressed in a mass-dependent manner owing to star formation-driven outflows (Davé et al. 2012). Once a galaxy’s halo mass is above about  $10^{12} M_{\odot}$ , its halo’s hot gas fraction is likely to be above 60% (Figure 1),

and its fuel supply for star-formation is cut off in our quenching model. In the simulations, as in observations (e.g. Peng et al. 2012), halo mass is tightly correlated with galaxy stellar mass for central galaxies. We show this relation in the top panels of Figure 4. The  $M_{\text{stellar}} - M_{\text{halo}}$  relation is tight for both blue and red centrals, but the slope differs for these two populations. For comparison, we also show observationally-inferred relations from Moster et al. (2010) and Behroozi et al. (2010).

Based on this correlation, a central galaxy with a halo mass of  $10^{12} M_{\odot}$  has a stellar mass of  $\approx 10^{10.5} M_{\odot}$ . Galaxies above this stellar mass tend to be quenched. Some central galaxies below this mass are also red; we address these in §3.9. Quenched galaxies above this stellar mass continue to grow via dry or semi-dry mergers (Gabor & Davé 2012), and they do so in such a way that maintains the correlation with halo mass – centrals in more massive halos accrete more stellar mass via mergers. We also note that these massive galaxies may accrete gas-rich satellites. This may lead to a brief “rejuvenation” of star-formation in the central galaxy such that it once again appears blue. Such cases are marked in the “blue centrals” (top left) panel of Figure 4 – these galaxies were previously quenched (for at least 3 consecutive snapshots) before becoming blue again. Though rare, these rejuvenated blue galaxies appear to follow the slope of *red* centrals in the  $M_{\text{stellar}} - M_{\text{halo}}$  relation, indicating that the rejuvenation does not lead to much stellar mass growth. The effective critical stellar mass  $\sim 10^{10.5} M_{\odot}$ ,

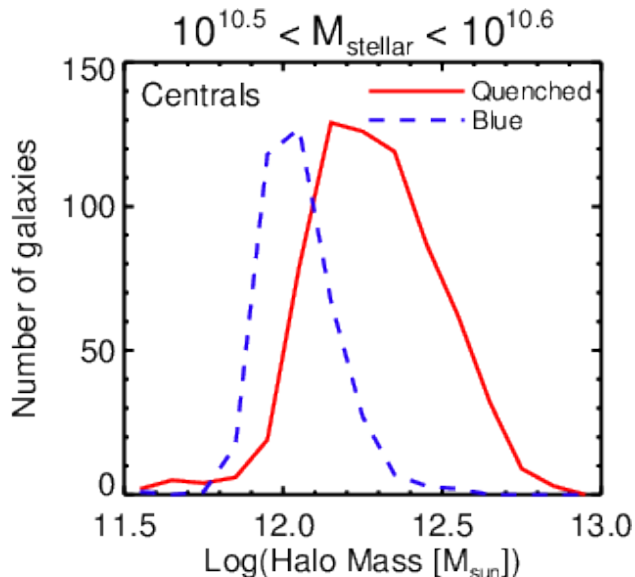


**Figure 5.** Distribution of halo masses for blue star-forming (blue dashed line) and quenched red (red solid line) central galaxies in a narrow range of stellar mass,  $10^{10.5} < M_{\text{stellar}} < 10^{10.6} M_{\odot}$ . At fixed stellar mass, quenched galaxies live in more massive halos.

where the  $M_{\text{stellar}} - M_{\text{halo}}$  relation changes slope, is closely related to the “knee” in the galaxy stellar mass function, as shown in Gabor & Davé (2012).

The presence of hot gas in massive halos therefore leads to the appearance of “mass quenching” among central galaxies: as galaxies grow more stellar mass, they also grow more halo mass; once they reach sufficiently high halo mass, they become hot gas-dominated; and in our quenching model, the hot gas quenches their star-formation. The efficiency of stellar mass growth (relative to the halo mass) decreases for these high mass galaxies because star-formation is suppressed.

In the bottom panels of Figure 4, we show the  $M_{\text{stellar}} - M_{\text{halo}}$  relation for blue and red satellites. For satellite galaxies, the stellar masses are essentially uncorrelated with halo masses. There is an upper envelope of stellar masses (there are no satellites towards the upper left of these panels) which arises simply because satellites cannot have masses larger than the centrals of their host halos (as pointed out in observational samples by Peng et al. 2012). Thus the stellar masses of satellite galaxies are mostly unrelated to their  $z = 0$  parent halo masses.

In summary, stellar masses are closely correlated with halo masses for central galaxies, but not for satellites. The slope of the  $M_{\text{stellar}} - M_{\text{halo}}$  relation for centrals changes at the characteristic quenching mass scale,  $M_{\text{halo}} \approx 10^{12} M_{\odot}$  or  $M_{\text{stellar}} \approx 10^{10.5} M_{\odot}$ .

### 3.3.1 At fixed $M_{\text{stellar}}$ , red central galaxies live in more massive halos than blue galaxies

In Figure 5 we show histograms of halo mass for blue and red central galaxies in a narrow range of stellar mass. This is like taking a narrow horizontal slice through the top panels of Figure 4, and plotting the halo mass distributions. We chose a mass range  $10^{10.5} < M_{\text{stellar}} < 10^{10.6} M_{\odot}$  because there are roughly equal numbers of blue and red centrals. This stellar mass is also near the “knee” in the simulated stellar mass function (Gabor & Davé 2012). The red galaxies live in significantly more massive halos than their

star-forming counterparts. This qualitatively agrees with clustering-based analyses, at least in the local universe (e.g. Tinker et al. 2013), and dynamical halo mass estimates (Phillips et al. 2014). This “bias” in halo masses at fixed stellar mass may help explain galactic conformity – the tendency for quenched centrals to have quenched satellites, and star-forming centrals to have star-forming satellites (Weinmann et al. 2006; Kauffmann et al. 2013; Robotham et al. 2013; Phillips et al. 2014). In our model, the quenched centrals live in more massive, hot halos, so their satellites are more likely to be quenched. We leave a more detailed analysis of galactic conformity for future work.

We can explain this effect physically two ways. (1) Immediately after a star-forming galaxy is quenched, its dark matter halo may continue to grow in mass while its stellar mass remains the same (ignoring galaxy mergers). (2) For main sequence star-forming galaxies, there is scatter in the  $M_{\text{stellar}} - M_{\text{halo}}$  relation. Those galaxies in the high-halo mass tail of this scatter are more likely to be quenched in our model. Thus the quenched galaxies will have higher halo mass. In practice both of these effects may combine to produce the difference in halo mass at fixed stellar mass.

Finally, we note (without showing in Figure 5) that this trend is reversed for low-mass central galaxies: for  $M_{\text{stellar}} < 10^{10} M_{\odot}$ , red galaxies actually live in less massive dark matter halos than their blue counterparts (though there are many more blue galaxies at these masses). As we explain in §3.9, such low-mass quenched central galaxies are predominantly ejected former satellites of much more massive halos. Thus their low halo masses could be explained by stripping of the dark matter halo through interaction with their former host halos.

## 3.4 Mass quenching independent of environment

Based on the boxy contour shape in Figure 2, mass quenching appears to be mostly independent of environment. In this section, we emphasize a simple explanation for this fact in light of our hot gas quenching model: hot halos (broadly, those with  $M_{\text{halo}} \gtrsim 10^{12} M_{\odot}$ ) occupy the full range of environments.

Although the critical halo mass for forming hot gas ( $10^{12} M_{\odot}$ ) is fairly large, such hot halos live in a wide variety of environments from the field to large groups. We show this visually in Figure 6 (using our  $24h^{-1}$  Mpc simulation for clarity). The left panel shows the cosmic web density, and the right panel shows gas temperature only for hot gas ( $> 10^{5.4}$  K). Over each image we plot the positions of red and blue galaxies (the size of each galaxy point is proportional to the square root of its stellar mass). As expected, the densest regions host lots of hot gas and red galaxies, while less dense filaments generally host star-forming galaxies. But some hot halos form in relatively isolated regions, as indicated in the figure. These isolated hot halos (which typically have masses just above  $10^{12} M_{\odot}$ ) generally host red galaxies.

For a more quantitative look, we show the relationship between parent halo mass and environment in Figure 7. For central galaxies, the correlation is poor except in the most extreme, massive halos. Around  $10^{12} M_{\odot}$ , central galaxy halos span nearly the full range of environments, so environment is not a good indicator of halo mass. This explains why mass quenching appears effectively independent of environment in both our simulations and in observations (Peng et al. 2010).

For satellite galaxies (lower panel of Figure 7) the relationship between parent halo mass and environment is more clear. Satellites living in massive groups are likely to have many nearby neighbors.

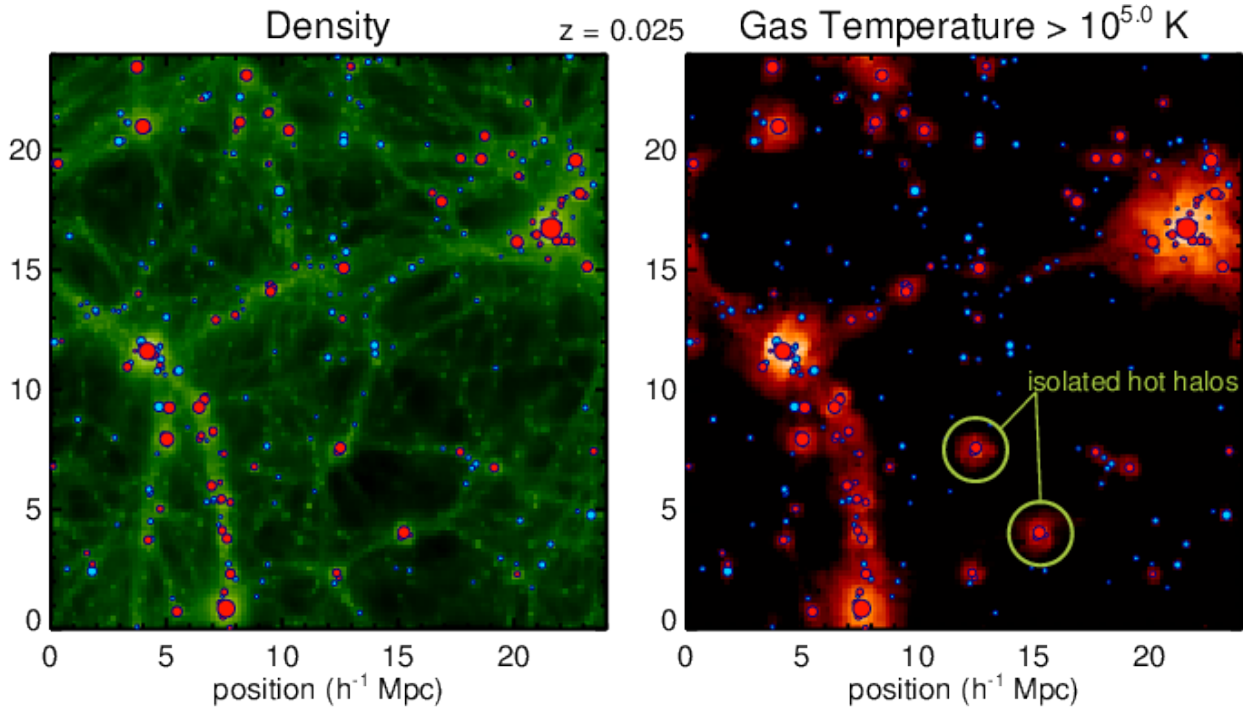


**Figure 6.** Density (left) and temperature (right) images of gas in the cosmic web, with galaxies overplotted as circles. The color of each point indicates whether the galaxy is red or blue, and the size of the circle scales with the square root of stellar mass. In the right panel, gas is only shown (in red scale) if it is hot ( $> 10^{5.4}$  K). Red galaxies tend to live in more clustered environments, but red centrals in hot halos are sometimes isolated. We highlight two examples of relatively isolated hot halos with large green circles.

Environment is therefore a reasonably good indicator of parent halo mass for satellites, although large scatter remains.

In summary, in our hot gas quenching model, halos around the critical quenching halo mass of  $10^{12} M_{\odot}$  live in the full range of environments. Thus environment is not a good indicator of parent halo mass for quenching halos, and mass quenching/central quenching appears to be independent of environment. Satellite galaxies, on the other hand, show a correlation between parent halo mass and environment.

### 3.5 Environment/Satellite quenching appears to be independent of $z = 0$ halo mass

While central galaxies are quenched when their halos become massive enough to support a hot atmosphere, two paths are possible for quenched satellite galaxies – 1) they are quenched as centrals before they become satellites, then merge into a larger halo, or 2) they are quenched as satellites by the hot gas existing in their parent halos. The second leads to the appearance of “environment quenching,” in which most galaxies in dense regions are red (cf. Figure 2). This satellite quenching mechanism is mostly independent of stellar mass because galaxies of all stellar masses may be satellites in quenching halos above  $10^{12} M_{\odot}$ .

Peng et al. (2012) noted that in SDSS data, environment or satellite quenching appears to be independent of the parent halo mass of satellite galaxies. In particular the knee,  $M^*$ , in the stellar mass function of blue satellite galaxies is independent of halo mass, and is the same as that for blue central galaxies. This indicates that blue satellites are subject to mass quenching at the same critical stellar mass, regardless of halo. These observed trends emerge

from our quenching model, despite the implicit dependence of quenching on halo mass (cf. Figure 1).

In the top panel of Figure 8 we show the stellar mass function of blue central galaxies. Symbols with error bars show the measured stellar mass function from our simulation (with arbitrary normalization). A single-Schechter fit to the blue central galaxies (shown as a solid line) yields a knee in the mass function of  $\log(M^*/M_{\odot}) = 10.18$ . This value for  $M^*$  is notably smaller than that in observations (cf. Peng et al. 2010; Ilbert et al. 2013; Moustakas et al. 2013) – our simulations likely produce too few massive blue galaxies (Gabor & Davé 2012), as noted in §2.1. Mass quenching sets this  $M^*$  cutoff because galaxies more massive than  $M^*$  are increasingly likely to live in massive ( $> 10^{12} M_{\odot}$ ), hot halos and thus be quenched.

In the bottom panel of Figure 8 we show stellar mass functions in 4 bins of parent halo mass. We choose the 4 halo bins to contain roughly the same number galaxies. When splitting the sample, the errorbars become substantial since the number of galaxies per bin is fairly small. Following Peng et al., we fit each stellar mass function with a single Schechter function with a power law slope fixed to  $-1.4$ . In these fits the normalization is arbitrary, and we allow  $M^*$  to vary. We find that the knee  $M^*$  shows no trend with halo mass, with all halo mass bins within 0.2 dex of the median  $\log(M^*/M_{\odot}) = 10.2$ .

In summary, mass quenching applies to satellite galaxies independent of parent halo mass. The stellar mass function “knee” (i.e. the critical quenching mass) for blue satellites is independent of halo mass, and it is the same as that for blue centrals. This independence on halo mass appears despite the close link with halo mass in our hot gas quenching model (cf. Figure 1). In the next section,

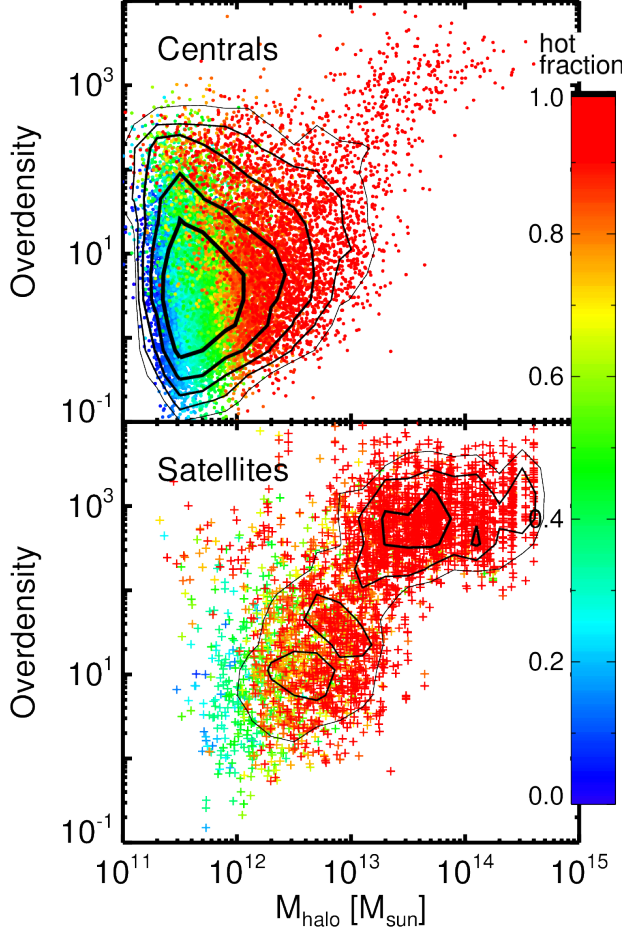


**Figure 7.** Environment vs. parent halo mass for central galaxies (top) and satellite galaxies (bottom). The color of each symbol indicates the hot gas fraction in the local vicinity of each galaxy. For centrals, environment is poorly correlated with halo mass, except in the rare, most massive halos. Thus halos with  $10^{12} < M_{\text{halo}} < 10^{13} M_{\odot}$ , which are generally dominated by hot gas, span nearly the full range of environments. Likewise, overdensity serves as a poor indicator of halo mass for centrals. For satellite galaxies the correlation between overdensity and halo mass is more clear, although with significant scatter.

we present a physical explanation for this – many satellite galaxies are pre-processed before entering their  $z = 0$  halos.

### 3.6 Pre-processing of satellite galaxies

How can a quenching process closely linked to halo mass lead to an apparent lack of dependence on halo mass? The answer is, through pre-processing – satellite galaxies in clusters at  $z = 0$  may have been pre-processed in groups at higher redshifts. Galaxies may assemble into groups at higher redshifts, and if their group masses are above  $\sim 10^{12} M_{\odot}$ , then they will be dominated by hot gas and begin quenching. Later, after the group galaxies have been quenched, the group may merge with a galaxy cluster. The group central galaxy, which has effectively been “mass quenched,” becomes a satellite galaxy of the cluster.

Several previous authors have studied pre-processing in simulations (Berrier et al. 2009; McGee et al. 2009; De Lucia et al. 2012). They typically identify galaxies in cluster-mass ha-

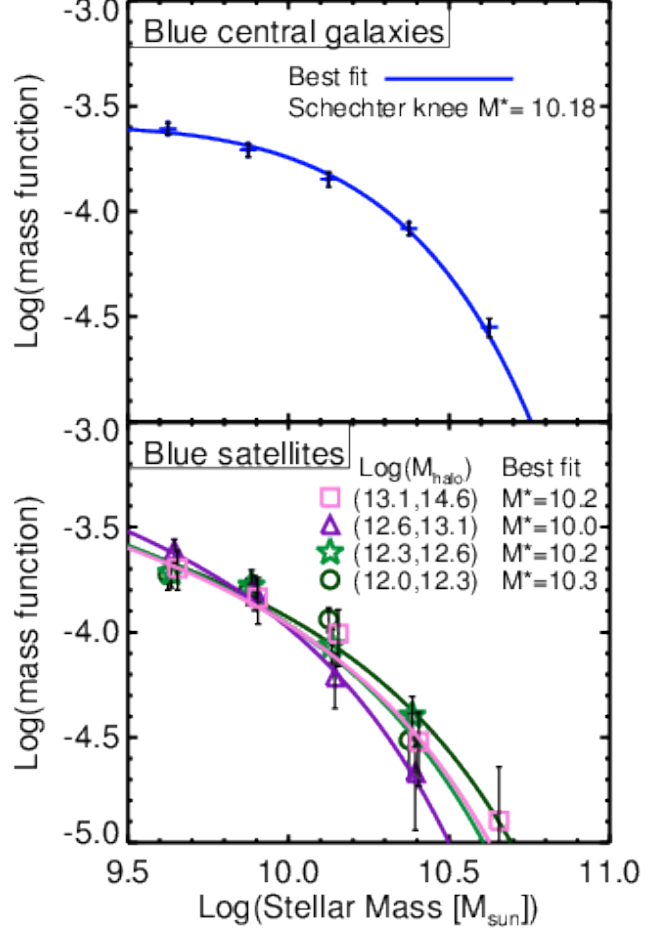


**Figure 8.** Stellar mass functions (number density of galaxies per logarithmic stellar mass bin) of blue centrals (top) and blue satellite galaxies in 4 bins of halo mass (chosen so that each bin has roughly the same number of galaxies, bottom). Symbols show the actual mass functions, while lines show Schechter function fits with the faint-end slope fixed to  $-1.4$  and the knee  $M^*$  free to vary (the normalization is arbitrary; Peng et al. 2012). The best-fit critical mass  $M^*$  shows no trend with halo mass, implying that mass quenching of satellite galaxies occurs independent of halo mass, as in observations.

los ( $> 10^{14} M_{\odot}$ ) that have been pre-processed in what we call massive groups, with  $M_{\text{halo}} > 10^{13} M_{\odot}$ . A more natural mass scale for pre-processing halos is that of “small groups,”  $M_{\text{halo}} = 10^{12} M_{\odot}$  (Williams et al. 2012). This is the mass scale where the virial shock forms a stable hot halo (cf. Figure 1), and in our simulations these are the halos where quenching begins. In what follows, we use  $10^{12} M_{\odot}$  as the pre-processing halo mass – galaxies in groups or clusters at  $z = 0$  may have been pre-processed in halos above  $10^{12} M_{\odot}$  at earlier epochs. This obviously includes the central galaxies of  $\sim 10^{12} M_{\odot}$  halos, which some authors consider field galaxies. Below we further define additional criteria to determine whether a galaxy has been pre-processed.

Figure 9 illustrates an example of pre-processing in our simulations. We show halo mass histories (top) and hot gas fraction histories (bottom) for two galaxies that end up in the same cluster at  $z = 0$ . One galaxy is pre-processed, while the other is not – it is a “late arrival” to the cluster environment. The pre-processed galaxy has lived in halos  $> 10^{12} M_{\odot}$  since before  $z = 1$ , and it lived in a

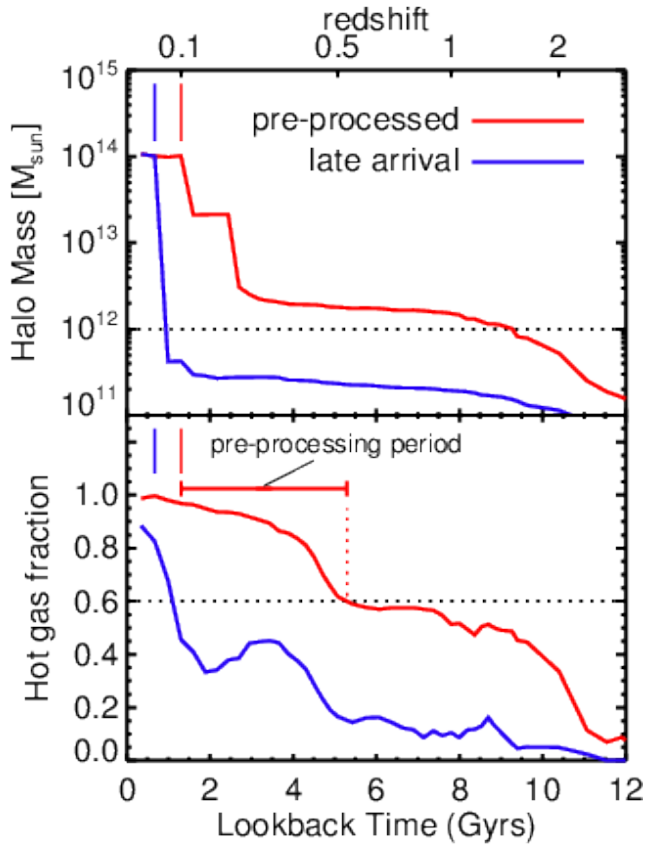


**Figure 9. Top:** Parent halo mass as a function of time for two galaxies that end up as satellites in the same galaxy cluster at  $z = 0$ . Short vertical lines (top left of each panel) indicate when each galaxy merged with the cluster. One galaxy is pre-processed in other halos with masses  $> 10^{12} M_{\odot}$  (red line), while the other lives only in low-mass halos (blue line) before joining the cluster. **Bottom:** Hot gas fraction (measured with the local subhalo) as a function of time for the same two galaxies. The pre-processed galaxy lives in a hot environment (above the critical hot fraction of 0.6, dotted line) starting at  $z \approx 0.5$  – it is pre-processed in this hot gas for about 4 Gyr before finally merging with the cluster at  $z \approx 0.1$ . The “late arrival” galaxy does not live in hot gas until it merges with the cluster.

hot gas-dominated halo since  $z \approx 0.5$ . Thus it was quenched well before joining the cluster. On the other hand, the late arrival galaxy lived only in low-mass, cold halos until joining the (hot) cluster at about 1 Gyr lookback time. At  $z = 0$ , although it accretes no new gas, this galaxy continues to form stars at a low level because it has not yet exhausted its supply of cold gas.

Based on halo mass and hot gas histories like these, we determine whether each satellite galaxy at  $z = 0$  was pre-processed. This requires tracing the halo mass history of each galaxy across cosmic time, as well as the full history of the halo in which the galaxy ends up at  $z = 0$ . We will refer to the latter – the  $z = 0$  host halo and its most massive progenitors – as the “main line” halo (this may be thought of as the “trunk” in a merger tree). Galaxies generally start out in distinct halos then merge with the “main line” halo to add to the cluster or group. A satellite is considered pre-processed if it satisfies the following three criteria: (1) at some time in the past, the galaxy lived in a halo distinct from the main line halo; (2) the parent halo just before merging with the main line halo had a lower mass than the main line halo, and a higher mass than  $10^{12} M_{\odot}$ ; (3)

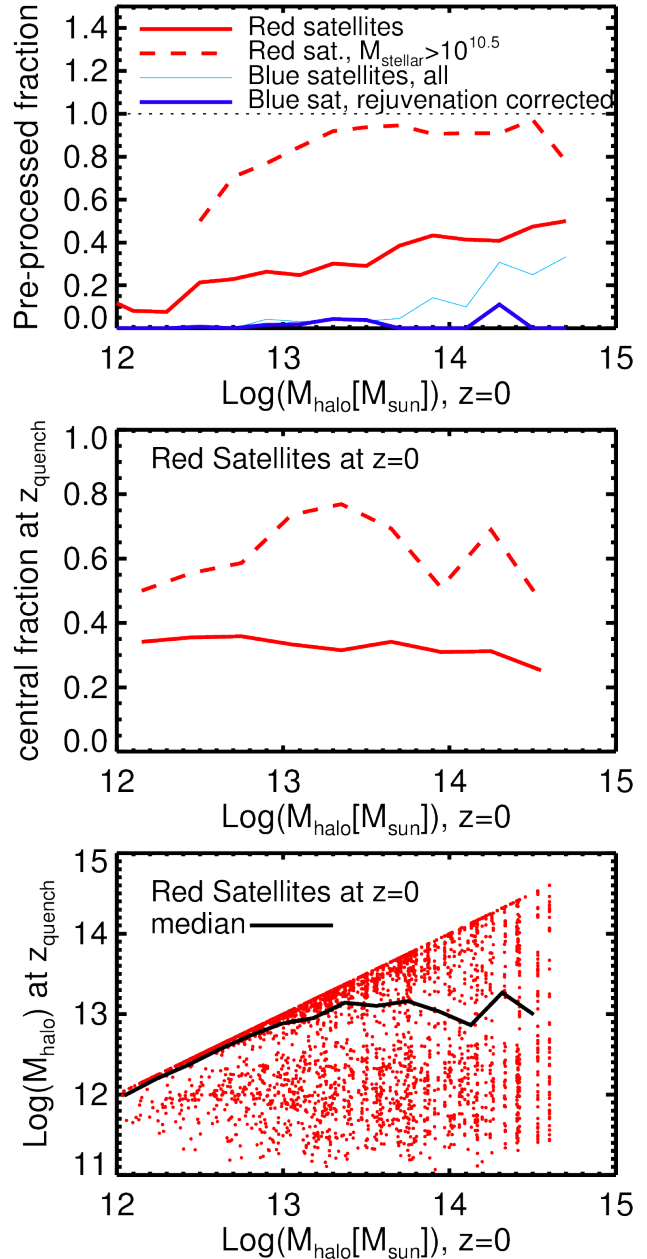


**Figure 10. Top:** Fraction of galaxies pre-processed in group-sized halos as a function of  $z = 0$  halo mass. In cluster-mass halos, roughly half of red satellites (solid red) and nearly all massive red satellites (dashed) were processed in groups before joining their  $z = 0$  halo. Most blue satellites (solid blue lines) that were pre-processed have actually been rejuvenated via gas-rich minor mergers – after excluding rejuvenated galaxies (thick, dark blue line), almost no blue satellites have been pre-processed. **Middle:** Fraction of  $z = 0$  satellite galaxies that were centrals at the redshift when they were quenched,  $z_{\text{quench}}$ , as a function of  $z = 0$  host halo mass. **Bottom:** Host halo mass of red satellites when they were quenched as a function of  $z = 0$  host halo mass. In the median, satellites in massive groups and clusters at  $z = 0$  lived in a halo of  $\sim 10^{13} M_{\odot}$  when they were first quenched (with a large scatter).

the galaxy lived in a hot gas-dominated environment for at least 1 Gyr prior to merging with the main line. These criteria ensure that the galaxy lived in a separate hot group before joining the final, larger group or cluster.

In the top panel of Figure 10 we show the fraction of satellites that were pre-processed as a function of  $z = 0$  parent halo mass. The pre-processed fraction of red satellite galaxies (solid red line) is a slowly increasing function of halo mass, ranging from 20 – 50 per cent. Roughly half of cluster satellites (i.e. in halos  $> 10^{14} M_{\odot}$ ) have been pre-processed before joining the cluster. This includes massive red satellites (approximately, above knee in the stellar mass function,  $M_{\text{stellar}} > 10^{10.5} M_{\odot}$ ), of which a vast majority were pre-processed.

The pre-processed fraction for blue satellites (blue lines) is very low. In cluster halos up to 30 per cent of blue satellites may be pre-processed, but most of these galaxies turn out to be rejuvenated galaxies – they were previously quenched, but they are forming stars because minor mergers with gas-rich satellites have provided a small amount of new fuel for star formation. Excluding rejuvenation (thick, dark blue line), a large majority of blue satellites have moved directly from “the field” to their final group or cluster environment. These blue galaxies are typically on their way to being fully quenched, but have not yet exhausted their fuel.

In the middle panel of Figure 10 we show the fraction of galaxies that were centrals at the time they were first quenched. We define  $z_{\text{quench}}$  as the highest redshift where a galaxy was red for at least two consecutive output snapshots. Roughly 30 per cent of  $z = 0$  red satellites were centrals when first quenched, including 50 – 75 per cent of massive red satellites. This means that most massive satellites were originally “mass quenched” in their own halos rather than “environment quenched” as satellites of a cluster.

In the bottom panel of Figure 10 we show, for red satellites, the parent halo mass at  $z_{\text{quench}}$  as a function of parent halo mass at  $z = 0$ . Especially for massive groups and clusters ( $M_{\text{halo}} > 10^{13} M_{\odot}$ ) at  $z = 0$ , a large fraction of red satellite galaxies lived in substantially lower-mass halos when they were first quenched.

In summary,  $\sim 20 - 50$  per cent of red satellite galaxies were pre-processed in lower-mass hot halos before joining their  $z = 0$  halo; most blue satellites were not pre-processed. Most massive red satellites (with  $M_{\text{stellar}} > 10^{10.5} M_{\odot}$ ) at  $z = 0$  were pre-processed as centrals galaxies at earlier times. This helps explain why satellite quenching does not show strong trends with halo mass – the knee in the mass function is largely set by “mass quenching” which occurs before the satellites arrive in their final halos.

### 3.7 Quenching and distance to the center of the parent halo

Based on observations, Woo et al. (2013) argue that distance from the halo center is a better predictor of quenching than environment for satellite galaxies. In Figure 11 we show the red fraction as a function of apparent projected distance from the halo center (normalized to the virial radius, i.e.  $D_{\text{gal}}/R_{\text{vir}}$ ) and halo mass. For massive groups and clusters in our simulations (halos with  $M_{\text{halo}} > 10^{13} M_{\odot}$ ), it turns out that a significant fraction of satellites are quenched even beyond  $1 R_{\text{vir}}$ . Thus, we include as “satellites” in this figure any galaxy that appears within two projected  $R_{\text{vir}}$ . If a galaxy is within the virial radius of two different halos, it is assigned to the more massive halo.

The resulting contours in Figure 11 show that the quenched fraction declines both as halo mass decreases and distance increases. These contours broadly match the shape of those in Figure

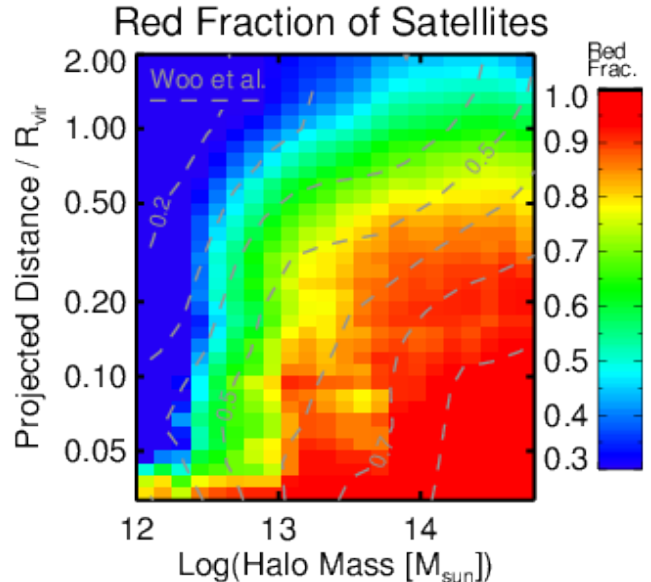


**Figure 11.** Red (i.e. quenched) fraction as a function of projected distance from the halo center and parent halo mass, for satellite galaxies. Here, we extend out to twice the virial radius, and count any galaxies within this doubled radius (in projection) as satellites. The shape of the contours is qualitatively similar to observations from Woo et al. (2013, grey dashed contours). In massive groups and clusters,  $\sim 50$  per cent of satellites are quenched at the virial radius. This suggests that the hot gas responsible for quenching extends beyond the virial radius.

10 of Woo et al. (2013), which we show here as grey dashed lines. In detail, the contours from our simulation lack some of the structure shown in the observations, and the simulated quenched fraction is higher overall. This suggests our quenching model is somewhat too efficient in these massive halos (as discussed in §2.1). In simulated massive groups and clusters, greater than half of satellite galaxies are quenched at the virial radius (which is probably too high; Wheeler et al. 2014), and many nearby galaxies are quenched even if they are beyond the virial radius. Nevertheless, the overall trend of quenching with halo mass and distance is striking, and qualitatively similar to that in observations (Wetzel et al. 2012).

In summary, satellite galaxies are more likely to be quenched when they are closer to their parent halo’s center, and when they live in more massive halos. In our models many galaxies are quenched beyond the virial radius of massive halos, and we further explore this effect below in §3.8.

#### 3.7.1 Radial positions of pre-processed galaxies

Now we briefly return to pre-processing and the joining of satellites into massive clusters and groups. In the top panel Figure 12 we show the pre-processed fraction as a function of distance from the halo center, for red satellites in massive groups and clusters with  $M_{\text{halo}} > 10^{13} M_{\odot}$ . The pre-processed fraction varies weakly with radius – even in cluster cores,  $> 30$  per cent of satellites are pre-processed. Some of these central pre-processed galaxies may have plunged toward the cluster center at late times, but many were pre-processed at high redshift before the bulk of the cluster assembled.

In the bottom panel of Figure 12, we show the lookback time at which each satellite merged into its final,  $z = 0$  halo, as a function of the distance from the halo center. As naively expected, galaxies at the outskirts of a group or cluster have merged with it more re-

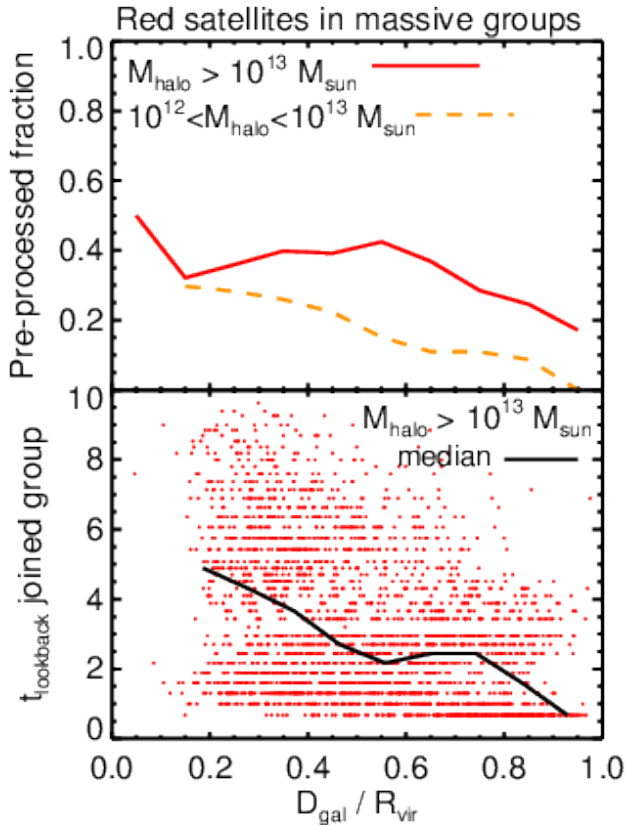


**Figure 12. Top:** Pre-processed fraction vs. distance (relative to  $R_{\text{vir}}$  for satellites in massive groups and clusters (halos above  $10^{13} M_{\odot}$ , solid line). The pre-processed fraction varies weakly with distance – galaxies near the centers of halos are just as likely as those at large radii to be pre-processed. Low-mass groups (dashed line) have fewer pre-processed satellites, and show a stronger radial gradient. **Bottom:** Lookback time (in Gyr) at which satellites joined their  $z = 0$  group or cluster (halos  $> 10^{13} M_{\odot}$ ), as a function of distance. Satellites near the edges of halos have typically joined more recently, although there is large scatter. Some galaxies near the centers of halos have merged with their host groups or clusters within the last 2 Gyr.

cently than those in the core. There is, however, a great deal of scatter, with many galaxies in cluster cores having joined the cluster within the last 2 Gyrs. Massive groups and clusters are dynamically complex, with some satellites able to plunge to the cluster core soon after merging with the halo.

### 3.8 Hot gas beyond the virial radius

An important implication of Figure 11 is that galaxies can be quenched well beyond the virial radius of a hot gas dominated halo (cf. Cybulski et al. 2014). There are two effects that contribute to this: First, there are ejected satellites, which we discuss further in §3.9. Here, we investigate how the hot gas around massive halos can extend to well beyond the virial radius.

Figure 13 shows radial temperature profiles (top panel), and the fraction of gas that is hot vs. radius (bottom panel) for halos of mass  $10^{12}$ ,  $10^{13}$ , and  $10^{14} M_{\odot}$ , out to  $5R_{\text{vir}}$ . For  $10^{12} M_{\odot}$  halos, the hot fraction normally drops below the critical value of 0.6 just beyond the virial radius, but for more massive halos the hot fraction remains high well beyond, to  $\approx 3R_{\text{vir}}$ . Cen (2011) and Bahé et al. (2013) note similar effects in their hydrodynamic simulations, in

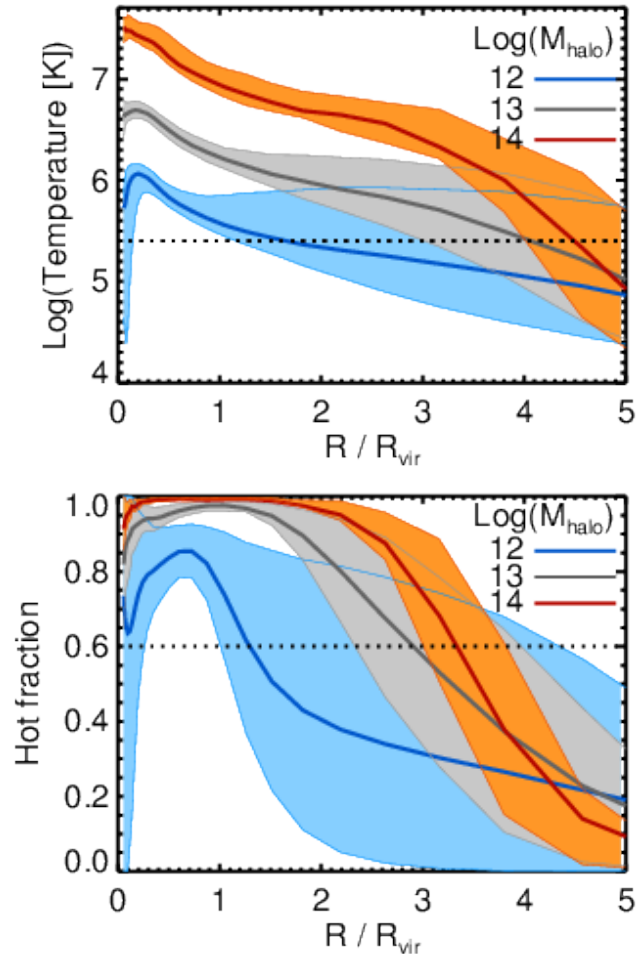


**Figure 13. Gas temperature (top) and hot gas fraction (bottom) vs. radius for halos of  $10^{12} M_{\odot}$  (blue),  $10^{13} M_{\odot}$  (grey), and  $10^{14} M_{\odot}$  (red). Dark lines show the mean temperature or hot fraction at that radius for all selected halos, while shading shows the  $1\sigma$  scatter. Dotted horizontal lines show the critical temperature we use to separate hot gas,  $10^{5.4} \text{ K}$  (top panel), and the critical hot fraction in our model, 0.6 (bottom panel).  $10^{12} M_{\odot}$  halos are hot out to  $\sim 1R_{\text{vir}}$ , while  $10^{13} M_{\odot}$  and  $10^{14} M_{\odot}$  halos are hot far beyond  $R_{\text{vir}}$ , out to  $3R_{\text{vir}}$ . The upper envelope of  $10^{12} M_{\odot}$  halos remain hot out to several  $R_{\text{vir}}$ , possibly because these halos are between  $1 - 3R_{\text{vir}}$  of more massive halos.**

which the hot gas beyond the virial radius also influences the gas content and star-formation of nearby galaxies (see also Behroozi et al. 2013, who show that dark matter sub-halos falling into massive host halos lose mass well before they reach their hosts' virial radii).

We have explicitly checked that hot gas extends beyond the virial radius even in simulations with no hot gas quenching and in a simulation with neither quenching nor stellar-driven galactic winds. These simulations, which were run at the same resolution and in  $48h^{-1} \text{ Mpc}$  boxes, show hot fraction and temperature profiles very similar to those in Figure 13. Combined with the fact that such extended hot gas is noted by other authors using different hydrodynamic methods and feedback prescriptions, this result suggests that virial shocks, rather than sub-grid physics, create the extra-halo hot gas. Hot gas beyond the virial radius is a general prediction of cosmological structure formation simulations.

We visually demonstrate hot gas beyond the virial radius in

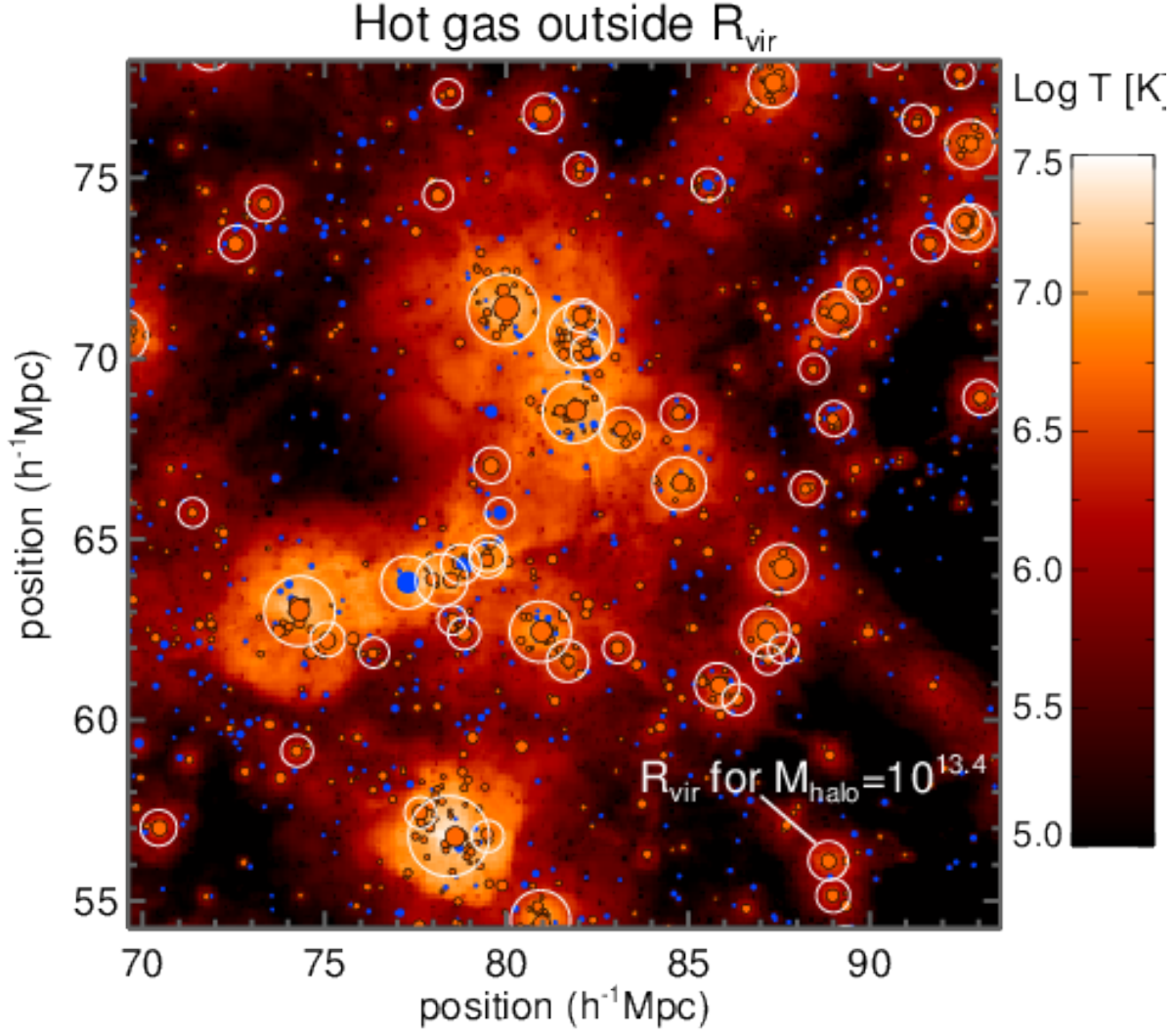


**Figure 14.** This image centered on a super-cluster demonstrates hot gas outside halos in our simulation. The background red-scale is the gas temperature. On top we plot red and blue filled circles for red and blue galaxies, respectively, where the size of the circle scales as  $\sqrt{M_{\text{stellar}}}$ . White (unfilled) circles show the virial radii for halos with  $M_{\text{halo}} > 10^{13} M_{\odot}$ . The most massive halo in this image ( $M_{\text{halo}} = 2 \times 10^{14} M_{\odot}$ ) appears near the bottom, just left of center.

Figure 14. Here we show a map of gas temperature only for gas with temperature  $T_{\text{gas}} > 10^{5.0}$  K, which appears as red-scale in the figure. We overplot blue and red galaxies in blue and red circles, with the size of the circle scaling with the square root of the stellar mass. Finally, white circles show the virial radii of halos with  $M_{\text{halo}} > 10^{13} M_{\odot}$ . In the lower right corner we indicate an example halo of mass  $10^{13.4} M_{\odot}$ . Hot gas clearly extends far beyond the virial radii of the most massive halos. It appears that the cosmic web forms super-structures where hot gas pervades the regions between adjacent groups and clusters.

In summary, gas around massive groups and clusters ( $M_{\text{halo}} > 10^{14} M_{\odot}$ ) remains hot out to  $\gtrsim 3R_{\text{vir}}$ . Hot gas pervades the regions between nearby groups and clusters, and can lead to environmental quenching effects beyond the virial radii of any massive halos. We quantify the importance of this form of quenching, which we call “neighborhood quenching,” in the next section.

### 3.9 Special case: Environment quenching of central galaxies, and ejected satellites

Figure 4 revealed a population of quenched central galaxies that live in halos with masses  $< 10^{12} M_{\odot}$ —we will call these low-mass red centrals. In the standard “halo quenching” picture where galaxies are quenched in halos  $> 10^{12} M_{\odot}$ , these galaxies should not be quenched (cf. Cattaneo et al. 2006). In our simulations, they are quenched for (at least) three different reasons: (1) there is scatter in the hot fraction –  $M_{\text{halo}}$  relation as shown in Figure 1, so that some halos slightly below  $10^{12} M_{\odot}$  are quenching halos; (2) some galaxies are “neighborhood quenched”: despite never having lived within the virial radius of a hot halo, they are affected by the hot gas that extends beyond the virial radius of massive halos (as shown in §3.8, and discussed in Bahé et al. 2013); (3) some galaxies are ejected former satellites of more massive halos, as discussed at length in Wetzel et al. (2013).

We disentangle these effects by identifying massive halos near the low-mass red central galaxies. For each low-mass red cen-

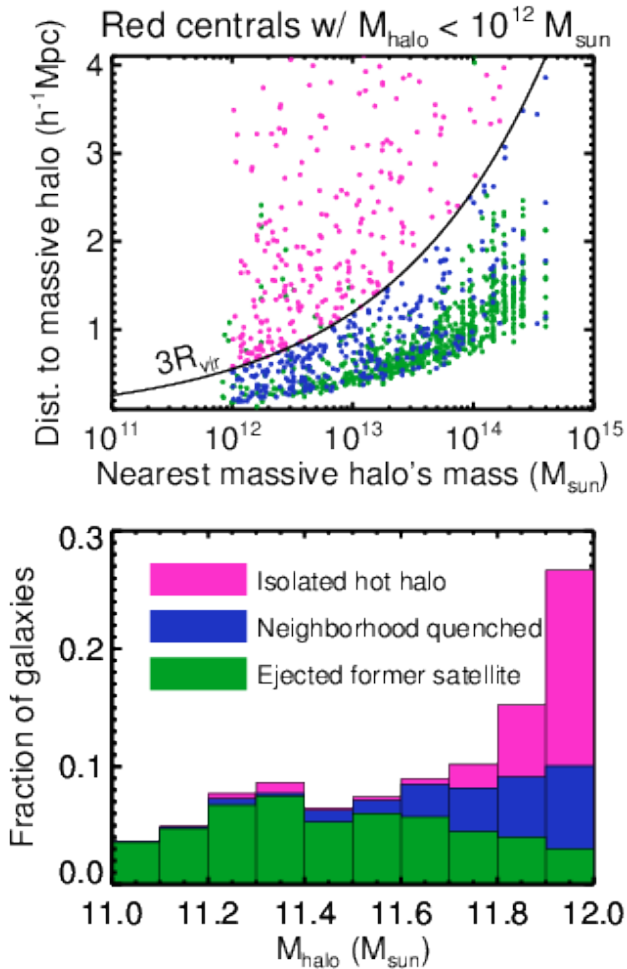


**Figure 15. Top:** Distance to the nearest massive halo vs. that halo’s mass, for quenched central galaxies with halo masses  $< 10^{12} M_{\odot}$  at  $z = 0$ . These galaxies are quenched despite their low halo masses because (1) they are truly isolated halos with masses just under  $10^{12} M_{\odot}$ , but they form hot halos owing to scatter in the hot gas fraction – halo mass relation (pink points); (2) they are neighborhood quenched by hot gas that extends beyond the virial radius of massive halos (blue points); or (3) they are ejected former satellites of massive halos (green points). We use the solid line marking  $3R_{\text{vir}}$  to distinguish isolated hot halos (above the line) from neighborhood quenched galaxies. **Bottom:** Histogram of actual halo masses for red galaxies with  $M_{\text{halo}} < 10^{12} M_{\odot}$ , with each bar in the histogram split by color depending on the galaxy’s status: truly isolated, neighborhood quenched, or ejected from a massive halo. Among red centrals with  $M_{\text{halo}} < 10^{12} M_{\odot}$ ,  $\sim 50\%$  are ejected satellites,  $\sim 20\%$  are neighborhood quenched, and  $\sim 30\%$  are isolated galaxies on the low-mass tail of the hot fraction vs.  $M_{\text{halo}}$  relation (cf. Figure 1).

tral galaxy at  $z = 0$ , we calculate a virial radius-scaled separation,  $S_R \equiv \Delta s/R_{\text{vir}}$ , from each halo with  $M_{\text{massive}} > 10^{12} M_{\odot}$ . Here  $\Delta s$  is the separation between the galaxy and the massive halo, and  $R_{\text{vir}}$  refers to the virial radius of the massive halo. We assign each galaxy (except ejected satellites; see below) to the massive halo for which  $S_R$  is smallest, and refer to this halo as the nearest massive halo.

We also identify galaxies as ejected satellites by considering their parent halo histories. If a galaxy previously lived in a halo more massive than its  $z = 0$  halo, and that previous halo had a mass  $> 10^{12} M_{\odot}$ , then we consider it an ejected satellite. In this case, we

find the most massive descendent of the previously hosting halo, and assign that as the nearest massive halo.

In the top panel of Figure 15, we show the distance to the nearest massive halo as a function of that halo’s mass, for these low-mass red centrals. We show ejected satellites in green, and split the remaining galaxies into neighborhood quenched (blue) and truly isolated (pink). To separate the latter two, we note from Figure 13 that hot gas typically dominates out to  $\sim 3R_{\text{vir}}$  for massive halos, and use this as a separator. After excluding ejected satellites, low-mass red centrals within  $3R_{\text{vir}}$  of their nearest massive halos are designated as neighborhood quenched, while those beyond  $3R_{\text{vir}}$  are considered truly isolated.

In the bottom panel of Figure 15, we show the distribution of actual halo masses for low-mass red centrals. Most of these low-mass red centrals have halo masses just below  $10^{12} M_{\odot}$ . We split each bar in the histogram by galaxy category, as above. About half of low-mass red centrals are ejected satellites,  $\sim 20$  per cent are neighborhood quenched, and  $\sim 30$  per cent are isolated. The distribution of isolated halos is strongly peaked towards higher masses, indicating that these form the low-mass tail of hot halos in the hot fraction- $M_{\text{halo}}$  distribution (shown in Figure 1). That is, these galaxies have formed their independent hot halos because they have masses close to, but below,  $10^{12} M_{\odot}$ .

To summarize, the population of quenched central galaxies with  $M_{\text{halo}} < 10^{12} M_{\odot}$  is roughly half ejected satellites, with a significant contribution from galaxies that are “neighborhood quenched” just because they live near massive, hot halos. About 30 per cent are isolated halos with sufficient mass to support their own hot coronae – these form the low-mass tail of hot halos on the hot gas fraction- $M_{\text{halo}}$  relation (shown in Figure 1).

## 4 DISCUSSION

### 4.1 A hot gas quenching narrative

Here we outline a quenching narrative that explains how galaxies are quenched under different circumstances. We consider galaxies whose  $z = 0$  *subhalo* masses end up at  $10^{14} M_{\odot}$ ,  $10^{13} M_{\odot}$ ,  $10^{12} M_{\odot}$ , and  $10^{11} M_{\odot}$ .

First consider a massive central galaxy in one of the highest density peaks of the cosmic web, destined to become the central galaxy in a massive cluster ( $M_{\text{halo}}(z = 0) > 10^{14} M_{\odot}$ ). Such a galaxy rapidly forms stars at high redshift, probably fueled by inflowing cold streams of gas. By  $z \approx 2$  this massive galaxy’s halo will become dominated by hot gas. The galaxy is strongly star-forming at the highest redshifts, but transitions to red and dead around  $z \sim 2$ , depending on the halo mass (Dekel et al. 2009; Oser et al. 2010). When its star formation shuts down, this galaxy will live in the center of a proto-cluster, and will remain quenched via some process that heats the surrounding hot gas. Thereafter, it will accrete additional stellar mass through mergers with satellite galaxies down to  $z = 0$ .

Next, consider the galaxies in two *subhalos* with final masses of  $10^{13} M_{\odot}$ : galaxy A in a highly overdense region near a cluster, galaxy B isolated. At high redshifts, both galaxies rapidly form stars, then their halos grow sufficiently large to support a hot halo and quenching begins around  $z \sim 1 - 2$ . This path is similar to that for the central cluster galaxy described above, but the quenching occurs later. After being quenched, galaxy A will eventually join a massive cluster, becoming a massive satellite within the cluster. It may grow in mass by continuing to accrete its own satellites even

after joining the cluster. Galaxy B remains isolated, becoming the central group galaxy of its own group. Both of these galaxies are mass quenched, but galaxy A ends up as a satellite.

Galaxies with final subhalo masses of  $\sim 10^{12} M_{\odot}$  have at least 5 different possible evolutionary histories. Galaxy I is in a relatively underdense environment. It evolves as a star-forming galaxy for most of cosmic history, then its halo becomes hot at low redshift and it appears as an isolated quenched galaxy at  $z = 0$ . Galaxy J is in a similarly underdense environment, but its halo remains dominated by cold gas until  $z = 0$ , simply because of the scatter in the hot gas fraction–halo mass relation (Figure 1) – there are halos slightly above  $10^{12} M_{\odot}$  that are never dominated by hot gas. Galaxy J thus remains as a star-forming galaxy throughout cosmic history. Galaxy K, on the other hand, lives in an overdense region. It evolves mostly like galaxy I, except that after quenching at low redshift, it joins a more massive halo and becomes a satellite galaxy. It is pre-processed in its own halo. Galaxy L joins a cluster before it is quenched by its own halo, so it is satellite quenched and remains at a lower stellar mass than galaxy K. Galaxy M joins a group before being quenched by its own halo – it is satellite quenched in the group – but then the host group merges with a cluster. Galaxy M is thus pre-processed as a satellite galaxy in a group before ending up in a cluster.

Finally, consider galaxies with final subhalo masses of  $\sim 10^{11} M_{\odot}$ . These generally take similar paths as the  $10^{12} M_{\odot}$  galaxies above, except that they are never quenched in isolation by their own halos. A small number may, however, be quenched in a massive group or cluster then be ejected from that halo, thus appearing as low-mass quenched centrals (cf. §3.9). It is also possible that they are “neighborhood quenched” simply by living *near* a massive hot halo whose hot gas extends well beyond its own virial radius.

These narratives illustrate the wide diversity of quenching histories. All are seen to occur in our simulations, arising from a simple criterion of preventing cold gas infall whenever the halo hot gas fraction exceeds 60%. Since so many different narratives occurring in a wide range of environments can lead to quenching of galaxies around  $10^{12} M_{\odot}$ , the natural consequence is that mass quenching is mostly independent of environment. Meanwhile, satellites that fall into or live near large halos are quenched, irrespective of their mass, which leads to the conclusion that environment (or more appropriately satellite) quenching is roughly independent of mass.

## 4.2 Galaxy structure in this quenching narrative

The narrative laid out above makes no mention of galaxy structure, morphology, or kinematics, despite that observations link these properties to quenching. Since our simulations cannot resolve thin stellar disks, they do not directly address the relationship between quenching and galaxy structure.

Quenched galaxies are generally bulge-dominated in the local universe, and recent work links central stellar density (Kauffmann et al. 2003, Fang et al. 2013 at low- $z$ ; and Franx et al. 2008, Cheung et al. 2012 at higher- $z$ ), stellar velocity dispersion (Bezanson et al. 2013), or bulge mass (Bluck et al. 2014) to quenching. This may suggest an important role for gas-rich major mergers, which commonly form classical bulges in idealized simulations (e.g. Barnes 1990; Hernquist et al. 1993; Robertson et al. 2006). But a substantial population of disk galaxies lives on the red sequence in both the local universe (Skibba et al. 2009; Masters et al. 2010) and at  $z > 1$  (Bundy et al. 2010; van der Wel et al. 2011; Bruce et al. 2013), and most quenched ellipticals show ordered rotation (Emsellem et al.

2007; Krajnović et al. 2011; Emsellem et al. 2011; though Cox et al. 2006 show that merger remnants may show ordered rotation).

So how could galaxy structure play into our hot gas quenching narrative? One intriguing possibility is that massive galaxies establish dense stellar cores at early times, before quenching. Halos in the high-redshift universe are thought to be denser than those today, and high-redshift ( $z \gtrsim 2$ ) star-forming galaxies may undergo disk instabilities (Noguchi 1999; Bournaud et al. 2007; Dekel et al. 2009; Ceverino et al. 2010) that help build observed dense star-forming bulges (Barro et al. 2013b,a; Williams et al. 2014). Perhaps after a starburst that exhausts their remaining dense gas, they quench in hot halos that starve them of fuel for star-formation. As their remaining disks fade and are harassed by close encounters in dense environments, they become strongly bulge-dominated in appearance (Carollo et al. 2013). After this, they may grow in stellar mass and size through mergers (Naab et al. 2009; Oser et al. 2012; Gabor & Davé 2012), with the details of their merger histories determining their final kinematics and internal structure (Naab et al. 2013). This scenario is essentially the one advocated by Dekel & Burkert (2013). Our simulations imply that later gas accretion must be prevented for such galaxies to remain red (Gabor et al. 2011); hot gas quenching is one such prevention mechanism that naturally leads to this scenario.

Gaseous mergers may also play a role in quenching, even if they are not solely responsible for it. Once a galaxy is starved of new fuel, it must rely on consuming its existing fuel to remain blue. If during this vulnerable stage it undergoes a merger, this can result in a rapid consumption of remaining gas (including the ejection of substantial cold gas in a molecular outflow; Walter et al. 2002; Narayanan et al. 2006, 2008; Feruglio et al. 2010; Sturm et al. 2011), thereby accelerating the transition to the red sequence. Hence in the hot gas quenching scenario, the role of gaseous mergers may be to set the *rapidity* of the transition to the red sequence. The most rapidly transitioning systems would appear as post-starburst galaxies (Quintero et al. 2004; Yang et al. 2008; Wild et al. 2009; Snyder et al. 2011), but galaxies that do not undergo such a merger would live as red disks for some time before their disk morphologies fade. Observations can constrain this dichotomy in quenching timescales (Schawinski et al. 2014), but simulating such morphological transitions together with quenching directly will require very high resolution in large volumes with representative galaxy samples – a challenge given current computational capabilities.

## 5 CONCLUSION

Using cosmological hydrodynamic simulations with a simple model for quenching star formation in massive halos dominated by hot gas, we have shown that hot gas drives both mass quenching and environment quenching. The model reproduces the crucial  $z = 0$  trends among quenching, stellar mass, halo mass, environment, and distance to the halo center. It also provides physical explanations for the observed trends. Key results are that:

- Our model reproduces the observed trend among red fraction, environment, and stellar mass that leads to the interpretation of separable mass quenching and environment quenching (Figure 2). Galaxies are increasingly likely to be quenched at high stellar masses and in dense environments. This trend emerges naturally from our hot gas fraction cut, or even a halo mass cut: galaxies are increasingly likely to be hosted by a halo with  $M_{\text{halo}} > 10^{12} M_{\odot}$  at high stellar masses and in dense environments.

- We also explicitly show that mass quenching mainly applies to central galaxies and environment quenching applies to satellite galaxies (Figure 3).

- The stellar mass – halo mass relation in our model matches observationally constrained abundance matching in the local universe (Figure 4), a key barometer that is difficult to achieve in current hydrodynamic simulations.

- Mass quenching appears independent of environment because halos with  $M_{\text{halo}} \sim 10^{12} M_{\odot}$ , where quenching begins, exist in a wide range of environments (Figures 2 and 7). This includes isolated “field” environments (Figure 6).

- Environment quenching appears independent of stellar and halo mass because galaxies in the densest environments uniformly live in hot halos with  $M_{\text{halo}} > 10^{12} M_{\odot}$ . Once a galaxy lives in such a hot halo, it will be quenched regardless of its stellar mass or host halo mass.

- Satellite galaxies show the effects of mass quenching, independent of their host halo mass (Figure 8). This is because massive galaxies that end up as satellites at  $z = 0$  are typically mass quenched in their own hot halos at higher redshift – a kind of pre-processing (cf. Figure 9).

- About 1/3 of red satellites were pre-processed, including  $\sim 90$  per cent of red satellites with  $M_{\text{stellar}} > 10^{10.5} M_{\odot}$ . About 2/3 of these massive red satellites were central galaxies when first quenched: they were mass quenched in their own hot halos, then joined larger halos to become satellites (Figure 10).

- Satellite galaxies are increasingly likely to be quenched at higher host halo masses and closer to the center of their host halos (Figure 11). This trend matches observations.

- Hot gas can extend far beyond the virial radii of massive halos, moreso for larger halos, reaching  $\sim 3 R_{\text{vir}}$  for clusters (Figures 13 and 14).

- Our model produces a population of red central galaxies that live in low-mass halos ( $M_{\text{halo}} < 10^{12} M_{\odot}$ ). These form through three main mechanisms: over half are ejected satellite galaxies that once lived in a more massive group or cluster hot halo; about 20 per cent are “neighborhood quenched”, embedded in the hot gas beyond the virial radius of a neighboring group or cluster; and about 30 per cent are truly isolated, arising from the scatter in the hot fraction – halo mass relation (Figure 15).

Our model outlines a plausible and simple scenario for the formation of quenched central and satellite galaxies in the nearby universe. It does not directly account for the morphology of galaxies, but including some simple considerations of morphological transformation owing to mergers, it seems at least qualitatively to accommodate a range of quenching paths from rapid quenching through a merger-induced post-starburst phase to a more gentle quenching via a red disk phase; in essence, the rapidity of quenching is set by the random chance of suffering a merger event, but the quenching itself is driven purely by the existence of a hot halo.

This heuristic model leaves many unanswered questions, of course. The main one is, what keeps the hot halo gas hot? The putative answer is AGN feedback, although the driving physics remains to be fully worked out. Another important consideration is the effect of galactic outflows during the star-forming phase that pumps metal-enriched (and thus more rapidly cooling) gas into the massive halo’s circumgalactic medium. Such outflows could potentially either add heat or enhance cooling (Kereš et al. 2009b), and could interact with inflowing filaments in ways that are difficult to model a priori (Kereš & Hernquist 2009) and difficult to understand analytically. There are also important redshift-dependent effects that

hot halos may be less effective at preventing accretion at earlier epochs (Dekel et al. 2009). Hence there remains much work to be done to sort out the physical drivers behind and cosmic evolution of hot gas quenching.

## ACKNOWLEDGEMENTS

We thank Joanna Woo for the observational data for Figure 11. We acknowledge Volker Springel for making GADGET publicly available, and thank the referee for helpful comments. JMG acknowledges support from the EC through grants ERC-StG-257720 and the CosmoComp ITN. Simulations were performed at TGCC and as part of a GENCI project (grants 2011-042192 and 2012-042192).

## REFERENCES

- Arnouts S., et al., 2007, *A&A*, 476, 137  
Bahé Y. M., McCarthy I. G., Balogh M. L., Font A. S., 2013, *MNRAS*, 430, 3017  
Barnes J. E., 1990, *Nature*, 344, 379  
Barro G., et al., 2013a, *arXiv:1311.5559*  
Barro G., et al., 2013b, *ApJ*, 765, 104  
Behroozi P. S., Conroy C., Wechsler R. H., 2010, *ApJ*, 717, 379  
Behroozi P. S., Wechsler R. H., Lu Y., Hahn O., Busha M. T., Klypin A., Primack J. R., 2013, *arXiv:1310.2239*  
Bell E. F., et al., 2004, *ApJ*, 608, 752  
Berrier J. C., Stewart K. R., Bullock J. S., Purcell C. W., Barton E. J., Wechsler R. H., 2009, *ApJ*, 690, 1292  
Bezanson R., van Dokkum P., van de Sande J., Franx M., Kriek M., 2013, *ApJ*, 764, L8  
Birnboim Y., Dekel A., 2003, *MNRAS*, 345, 349  
Birnboim Y., Dekel A., 2011, *MNRAS*, 415, 2566  
Birnboim Y., Dekel A., Neistein E., 2007, *MNRAS*, 380, 339  
Blanton M. R., Moustakas J., 2009, *ARA&A*, 47, 159  
Blanton M. R., et al., 2005, *AJ*, 129, 2562  
Bluck A. F. L., Mendel J. T., Ellison S. L., Moreno J., Simard L., Patton D. R., Starkenburg E., 2014, *arXiv:1403.5269*  
Bournaud F., Elmegreen B. G., Elmegreen D. M., 2007, *ApJ*, 670, 237  
Bower R. G., Benson A. J., Malbon R., Helly J. C., Frenk C. S., Baugh C. M., Cole S., Lacey C. G., 2006, *MNRAS*, 370, 645  
Brammer G. B., et al., 2009, *ApJ*, 706, L173  
Brammer G. B., et al., 2011, *ApJ*, 739, 24  
Bruce V. A., et al., 2013, *arXiv:1301.6373*  
Bruzual G., Charlot S., 2003, *MNRAS*, 344, 1000  
Bundy K., et al., 2010, *ApJ*, 719, 1969  
Carollo C. M., et al., 2013, *ApJ*, 773, 112  
Cattaneo A., Dekel A., Devriendt J., Guiderdoni B., Blaizot J., 2006, *MNRAS*, 370, 1651  
Cen R., 2011, *ApJ*, 741, 99  
Ceverino D., Dekel A., Bournaud F., 2010, *MNRAS*, 404, 2151  
Cheung E., et al., 2012, *ApJ*, 760, 131  
Conroy C., et al., 2007, *ApJ*, 654, 153  
Cooper M. C., Newman J. A., Madgwick D. S., Gerke B. F., Yan R., Davis M., 2005, *ApJ*, 634, 833  
Cooper M. C., et al., 2006, *MNRAS*, 370, 198  
Cooper M. C., et al., 2007, *MNRAS*, 376, 1445  
Cox T. J., Dutta S. N., Di Matteo T., Hernquist L., Hopkins P. F., Robertson B., Springel V., 2006, *ApJ*, 650, 791

- Croton D. J., et al., 2006, *MNRAS*, 365, 11
- Cybulski R., Yun M. S., Fazio G. G., Gutermuth R. A., 2014, *MNRAS*, 439, 3564
- Davé R., Finlator K., Oppenheimer B. D., 2007, in E. Emsellem, H. Wozniak, G. Massacrier, J.-F. Gonzalez, J. Devriendt, & N. Champavert ed., *EAS Publications Series Vol. 24*, *EAS Publications Series*. pp 183–189, doi:10.1051/eas:2007026
- Davé R., Oppenheimer B. D., Sivanandam S., 2008, *MNRAS*, 391, 110
- Davé R., Oppenheimer B. D., Katz N., Kollmeier J. A., Weinberg D. H., 2010, *MNRAS*, 408, 2051
- Davé R., Oppenheimer B. D., Finlator K., 2011a, *MNRAS*, 415, 11
- Davé R., Finlator K., Oppenheimer B. D., 2011b, *MNRAS*, 416, 1354
- Davé R., Finlator K., Oppenheimer B. D., 2012, *MNRAS*, 421, 98
- De Lucia G., Boylan-Kolchin M., Benson A. J., Fontanot F., Monaco P., 2010, *MNRAS*, 406, 1533
- De Lucia G., Weinmann S., Poggianti B. M., Aragón-Salamanca A., Zaritsky D., 2012, *MNRAS*, 423, 1277
- Dekel A., Birnboim Y., 2006, *MNRAS*, 368, 2
- Dekel A., Birnboim Y., 2008, *MNRAS*, 383, 119
- Dekel A., Burkert A., 2013, *MNRAS*,
- Dekel A., Sari R., Ceverino D., 2009, *ApJ*, 703, 785
- Dressler A., 1980, *ApJ*, 236, 351
- Elbaz D., et al., 2007, *A&A*, 468, 33
- Emsellem E., et al., 2007, *MNRAS*, 379, 401
- Emsellem E., et al., 2011, *MNRAS*, 414, 888
- Faber S. M., et al., 2007, *ApJ*, 665, 265
- Fabian A. C., Nulsen P. E. J., Canizares C. R., 1984, *Nature*, 310, 733
- Fang J. J., Faber S. M., Koo D. C., Dekel A., 2013, *ApJ*, 776, 63
- Feldmann R., Carollo C. M., Mayer L., 2011, *ApJ*, 736, 88
- Feruglio C., Maiolino R., Piconcelli E., Menci N., Aussel H., Lamastra A., Fiore F., 2010, *A&A*, 518, L155+
- Finlator K., Davé R., 2008, *MNRAS*, 385, 2181
- Finlator K., Davé R., Papovich C., Hernquist L., 2006, *ApJ*, 639, 672
- Finlator K., Davé R., Oppenheimer B. D., 2007, *MNRAS*, 376, 1861
- Franx M., van Dokkum P. G., Schreiber N. M. F., Wuyts S., Labbé I., Toft S., 2008, *ApJ*, 688, 770
- Gabor J. M., Davé R., 2012, *MNRAS*, 427, 1816
- Gabor J. M., Davé R., Finlator K., Oppenheimer B. D., 2010, *MNRAS*, 407, 749
- Gabor J. M., Davé R., Oppenheimer B. D., Finlator K., 2011, *MNRAS*, 417, 2676
- Gunn J. E., Gott J. R. I., 1972, *ApJ*, 176, 1
- Haardt F., Madau P., 2001, in D. M. Neumann & J. T. V. Tran ed., *Clusters of Galaxies and the High Redshift Universe Observed in X-rays*. [arXiv:astro-ph/0106018](https://arxiv.org/abs/astro-ph/0106018)
- Hayward C. C., Torrey P., Springel V., Hernquist L., Vogelsberger M., 2014, *MNRAS*, 442, 1992
- Hernquist L., Spergel D. N., Heyl J. S., 1993, *ApJ*, 416, 415
- Hopkins P. F., 2013, *MNRAS*, 428, 2840
- Hopkins P. F., Hernquist L., Cox T. J., Di Matteo T., Robertson B., Springel V., 2006, *ApJS*, 163, 1
- Hopkins P. F., Cox T. J., Kereš D., Hernquist L., 2008, *ApJS*, 175, 390
- Ilbert O., et al., 2013, *A&A*, 556, A55
- Johansson P. H., Naab T., Ostriker J. P., 2009, *ApJ*, 697, L38
- Kauffmann G., et al., 2003, *MNRAS*, 341, 54
- Kauffmann G., Li C., Zhang W., Weinmann S., 2013, *MNRAS*, 430, 1447
- Kennicutt Jr. R. C., 1998, *ApJ*, 498, 541
- Kereš D., Hernquist L., 2009, *ApJ*, 700, L1
- Kereš D., Katz N., Weinberg D. H., Davé R., 2005, *MNRAS*, 363, 2
- Kereš D., Katz N., Fardal M., Davé R., Weinberg D. H., 2009a, *MNRAS*, 395, 160
- Kereš D., Katz N., Davé R., Fardal M., Weinberg D. H., 2009b, *MNRAS*, 396, 2332
- Kereš D., Vogelsberger M., Sijacki D., Springel V., Hernquist L., 2012, *MNRAS*, 425, 2027
- Knobel C., et al., 2013, *ApJ*, 769, 24
- Komatsu E., et al., 2009, *ApJS*, 180, 330
- Kovač K., et al., 2010, *ApJ*, 708, 505
- Krajnović D., et al., 2011, *MNRAS*, 414, 2923
- Leauthaud A., et al., 2012a, *ApJ*, 744, 159
- Leauthaud A., et al., 2012b, *ApJ*, 746, 95
- Mandelbaum R., Seljak U., Kauffmann G., Hirata C. M., Brinkmann J., 2006, *MNRAS*, 368, 715
- Martin C. L., 2005, *ApJ*, 621, 227
- Masters K. L., et al., 2010, *MNRAS*, 405, 783
- Mathews W. G., 2009, *ApJ*, 695, L49
- McGee S. L., Balogh M. L., Bower R. G., Font A. S., McCarthy I. G., 2009, *MNRAS*, 400, 937
- McKee C. F., Ostriker J. P., 1977, *ApJ*, 218, 148
- Moster B. P., Somerville R. S., Maulbetsch C., van den Bosch F. C., Macciò A. V., Naab T., Oser L., 2010, *ApJ*, 710, 903
- Moustakas J., et al., 2013, *ApJ*, 767, 50
- Murray N., Quataert E., Thompson T. A., 2005, *ApJ*, 618, 569
- Murray N., Ménard B., Thompson T. A., 2011, *ApJ*, 735, 66
- Muzzin A., et al., 2013, *ApJ*, 777, 18
- Naab T., Johansson P. H., Ostriker J. P., 2009, *ApJ*, 699, L178
- Naab T., et al., 2013, [arXiv:1311.0284](https://arxiv.org/abs/1311.0284)
- Narayanan D., et al., 2006, *ApJ*, 642, L107
- Narayanan D., et al., 2008, *ApJS*, 176, 331
- Nelson D., Vogelsberger M., Genel S., Sijacki D., Kereš D., Springel V., Hernquist L., 2013, *MNRAS*, 429, 3353
- Noguchi M., 1999, *ApJ*, 514, 77
- Oppenheimer B. D., Davé R., 2006, *MNRAS*, 373, 1265
- Oppenheimer B. D., Davé R., 2008, *MNRAS*, 387, 577
- Oppenheimer B. D., Davé R., 2009, *MNRAS*, 395, 1875
- Oppenheimer B. D., Davé R., Finlator K., 2009, *MNRAS*, 396, 729
- Oppenheimer B. D., Davé R., Katz N., Kollmeier J. A., Weinberg D. H., 2012, *MNRAS*, 420, 829
- Oser L., Ostriker J. P., Naab T., Johansson P. H., Burkert A., 2010, *ApJ*, 725, 2312
- Oser L., Naab T., Ostriker J. P., Johansson P. H., 2012, *ApJ*, 744, 63
- Peng Y.-j., et al., 2010, *ApJ*, 721, 193
- Peng Y.-j., Lilly S. J., Renzini A., Carollo M., 2012, *ApJ*, 757, 4
- Phillips J. I., Wheeler C., Boylan-Kolchin M., Bullock J. S., Cooper M. C., Tollerud E. J., 2014, *MNRAS*, 437, 1930
- Quadri R. F., Williams R. J., Franx M., Hildebrandt H., 2012, *ApJ*, 744, 88
- Quintero A. D., et al., 2004, *ApJ*, 602, 190
- Robertson B., Cox T. J., Hernquist L., Franx M., Hopkins P. F., Martini P., Springel V., 2006, *ApJ*, 641, 21
- Robotham A. S. G., et al., 2013, *MNRAS*, 431, 167
- Rupke D. S., Veilleux S., Sanders D. B., 2005, *ApJS*, 160, 115
- Saitoh T. R., Makino J., 2013, *ApJ*, 768, 44

- Scannapieco E., Bildsten L., 2005, *ApJ*, 629, L85
- Schawinski K., et al., 2014, *MNRAS*, 440, 889
- Skibba R. A., et al., 2009, *MNRAS*, 399, 966
- Snyder G. F., Cox T. J., Hayward C. C., Hernquist L., Jonsson P., 2011, *ApJ*, 741, 77
- Somerville R. S., Hopkins P. F., Cox T. J., Robertson B. E., Hernquist L., 2008, *MNRAS*, 391, 481
- Springel V., 2005, *MNRAS*, 364, 1105
- Springel V., 2010, *MNRAS*, 401, 791
- Springel V., Hernquist L., 2003, *MNRAS*, 339, 289
- Straatman C. M. S., et al., 2013, [arXiv:1312.4952](#)
- Strateva I., et al., 2001, *AJ*, 122, 1861
- Sturm E., et al., 2011, *ApJ*, 733, L16
- Sutherland R. S., Dopita M. A., 1993, *ApJS*, 88, 253
- Tinker J. L., Leauthaud A., Bundy K., George M. R., Behroozi P., Massey R., Rhodes J., Wechsler R. H., 2013, *ApJ*, 778, 93
- Torrey P., Vogelsberger M., Genel S., Sijacki D., Springel V., Hernquist L., 2014, *MNRAS*,
- Vogelsberger M., Sijacki D., Kereš D., Springel V., Hernquist L., 2012, *MNRAS*, 425, 3024
- Vogelsberger M., Genel S., Sijacki D., Torrey P., Springel V., Hernquist L., 2013, *MNRAS*, 436, 3031
- Walter F., Weiss A., Scoville N., 2002, *ApJ*, 580, L21
- Weinmann S. M., van den Bosch F. C., Yang X., Mo H. J., 2006, *MNRAS*, 366, 2
- Wetzel A. R., Tinker J. L., Conroy C., 2012, *MNRAS*, 424, 232
- Wetzel A. R., Tinker J. L., Conroy C., van den Bosch F. C., 2013, [arXiv:1303.7231](#)
- Wheeler C., Phillips J. I., Cooper M. C., Boylan-Kolchin M., Bullock J. S., 2014, [arXiv:1402.1498](#)
- Whitaker K. E., et al., 2013, *ApJ*, 770, L39
- Wild V., Walcher C. J., Johansson P. H., Tresse L., Charlot S., Pollo A., Le Fèvre O., de Ravel L., 2009, *MNRAS*, 395, 144
- Williams R. J., Quadri R. F., Franx M., van Dokkum P., Labbé I., 2009, *ApJ*, 691, 1879
- Williams R. J., Kelson D. D., Mulchaey J. S., Dressler A., McCarthy P. J., Shectman S. A., 2012, *ApJ*, 749, L12
- Williams C. C., et al., 2014, *ApJ*, 780, 1
- Woo J., et al., 2013, *MNRAS*, 428, 3306
- Yang Y., Zabludoff A. I., Zaritsky D., Mihos J. C., 2008, *ApJ*, 688, 945
- van der Wel A., et al., 2011, *ApJ*, 730, 38